HHS Public Access

Author manuscript

Nature. Author manuscript; available in PMC 2015 April 23.

Published in final edited form as:

Nature. 2014 October 23; 514(7523): 455–461. doi:10.1038/nature13808.

Structure and immune recognition of trimeric prefusion HIV-1 Env

Marie Pancera[1], **Tongqing Zhou**[1], **Aliaksandr Druz**[1], **Ivelin S. Georgiev**[1], **Cinque Soto**[1], **Jason Gorman**[1], **Jinghe Huang**[2], **Priyamvada Acharya**[1], **Gwo-Yu Chuang**[1], **Gilad Ofek**[1], **Guillaume B. E. Stewart-Jones**[1], **Jonathan Stuckey**[1], **Robert T. Bailer**[1], **M. Gordon Joyce**[1], **Mark K. Louder**[1], **Nancy Tumba**[3], **Yongping Yang**[1], **Baoshan Zhang**[1], **Myron S. Cohen**[4], **Barton F. Haynes**[5], **John R. Mascola**[1], **Lynn Morris**[3], **James B. Munro**[6], **Scott C. Blanchard**[7], **Walther Mothes**[6], **Mark Connors**[2], and **Peter D. Kwong**[1,*]

[1] Vaccine Research Center, Laboratory of Immunoregulation, National Institute of Allergy and Infectious Diseases, National Institutes of Health, Bethesda, Maryland 20892, USA.

[2] HIV-Specific Immunity Section, Laboratory of Immunoregulation, National Institute of Allergy and Infectious Diseases, National Institutes of Health, Bethesda, Maryland 20892, USA.

[3] Center for HIV and STIs, National Institute for Communicable Diseases of the National Health Laboratory Service (NHLS), and University of the Witwatersrand, Johannesburg, South Africa, and Centre for the AIDS Programme of Research in South Africa (CAPRISA), University of KwaZulu-Natal, Durban, South Africa.

[4] Departments of Medicine, Epidemiology, Microbiology and Immunology, University of North Carolina at Chapel Hill, Chapel Hill, North Carolina 27599, USA.

[5] Duke University Human Vaccine Institute, Departments of Medicine, Surgery, Pediatrics and Immunology, Duke University School of Medicine, and the Center for HIV/AIDS Vaccine Immunology-Immunogen Discovery at Duke University, Durham, North Carolina 27710, USA.

[6] Department of Microbial Pathogenesis, Yale University School of Medicine, New Haven, Connecticut 06536, USA.

[7] Department of Physiology and Biophysics, Weill Cornell Medical College of Cornell University, New York, New York 10021, USA.

* To whom correspondence should be addressed: pdkwong@nih.gov (P.D.K.).

Author Contributions MP, TZ, AD and PDK determined the trimer structure, with MP heading structure determination, TZ assisting with solution and refinement, AD with protein production, and PDK with data collection. ISG and CS performed bioinformatics analysis, JG conformational analysis, PA, GYC, GO, GSJ and JS antigenic and mechanistic analyses, RTB, MGJ, MKL, NT, YY, BZ, MSC, BFH, JRM, and LM cohort analysis, JBM, SCB and WM smFRET analysis, and JH and MC provided antibody 35O22. MP and PDK wrote the paper, on which all principal investigators commented.

Author Information Coordinates and structure factors for BG505 SOSIP.664 in complex with PGT122 and 35O22 Fabs have been deposited with the Protein Data Bank under accession code 4TVP. The authors declare no competing financial interests.

Figures

Structure figures were prepared using PYMOL[81]. PDB IDs are referenced throughout except for 2HMG[82], 1QU1[83], 4MMU[47], 3RRT[37], 3CSY[39] and 2EBO[84] in Figure 4; 2YP7[85] and 4JHW[31] in Figures 5 and 6 and PDB ID: 3HI1[86] in Extended Data Table 2.

Interfaces

Interactive surfaces were obtained from PISA (www.ebi.ac.uk/pdbe/pisa/).

Abstract

The HIV-1-envelope (Env) spike, comprising three gp120 and three gp41 subunits, is a conformational machine that facilitates HIV-1 entry by rearranging from a mature unliganded state, through receptor-bound intermediates, to a postfusion state. As the sole viral antigen on the HIV-1-virion surface, Env is both the target of neutralizing antibodies and a focus of vaccine efforts. Here we report the structure at 3.5-Å resolution for an HIV-1-Env trimer captured in a mature closed state by antibodies PGT122 and 35O22. This structure reveals the prefusion conformation of gp41, indicates rearrangements needed for fusion activation, and defines parameters of immune evasion and immune recognition. Prefusion gp41 encircles N- and C-terminal strands of gp120 with four helices that form a membrane-proximal collar, fastened by insertion of a fusion peptide-proximal methionine into a gp41-tryptophan clasp. Spike rearrangements required for entry likely involve opening the clasp and expelling the termini. *N*-linked glycosylation and sequence-variable regions cover the prefusion closed spike: we used chronic cohorts to map the prevalence and location of effective HIV-1-neutralizing responses, which were distinguished by their recognition of *N*-linked glycan and tolerance for epitope-sequence variation.

Over the last 50 years, more than 70 million people have been infected or killed by the human immunodeficiency virus type 1 (HIV-1)[1]. A dominant contributing factor has been the biochemical complexity and conformational dynamics of the HIV-1-envelope (Env) spike, a type I fusion machine that facilitates virus entry into cells by interacting with host cellular receptors and fusing membranes of virus and host cell (reviewed in [2]). Despite its exposed position on the viral membrane and the generation of narrow-breadth neutralizing antibody responses throughout the course of HIV-1 infection, the evolving HIV-1-Env spike successfully evades most antibody-mediated neutralization[3]. This evasion is, to a large degree, responsible for the difficulty in developing an effective HIV-1 vaccine.

Initially synthesized as a gp160 precursor, which is cleaved into gp120 and gp41 subunits, the trimeric HIV-1-Env spike displays unusual posttranslational processing including the addition of 25-30 *N*-linked glycans per gp120-gp41 protomer[4], tyrosine sulfation[5], and slow signal peptide cleavage[6]. Env rearranges from a prefusion mature closed state that evades antibody recognition through intermediate open states that bind to receptors, CD4 and co-receptor (either CCR5 or CXCR4), to a postfusion state (reviewed in [2]). Over the last 20 years, substantial atomic-level detail has been obtained on these states, including structures of receptor-bound gp120[7], postfusion gp41[8,9], and most recently the trimeric arrangement of prefusion gp120 along with two gp41 helices, one of which was aligned in sequence[10,11]. The prefusion structure of gp41 has, however, resisted atomic-level analysis. Because the primary structural rearrangement driving membrane fusion is the gp41 transition from prefusion to postfusion conformations, the lack of a prefusion gp41 structure has stymied attempts to provide a coherent picture of the conformational rearrangements the spike undergoes to facilitate entry.

Here we use neutralizing antibodies PGT122[12] and 35O22[13] to capture the HIV-1 spike in a prefusion mature closed state. We obtained crystals of the antigen-binding fragments (Fabs) of these two antibodies in complex with a soluble, cleaved, Env trimer construct (BG505

SOSIP.664)[14-16] and determined its atomic-level structure. Examination of this structure in the context of previously determined gp120 and gp41 structures affords a mechanistic understanding of the conformational transitions the spike undergoes to facilitate virus entry. We delineated aggregate parameters of glycan shielding and genetic variation and used infected donor serum to determine where the immune system succeeds in recognizing the HIV-1 spike. Analysis of the prefusion HIV-1-Env structure and its conformational rearrangements, combined with an understanding of its evasion from and vulnerabilities to the immune system, reveal similarities to other type I viral fusion machines as well as features of recognition by the human immune system unique to this critical vaccine target.

Structure determination and overall structure

Atomic-level information for virtually all of the HIV-1-Env ectodomain in its prefusion conformation has been obtained from antibody-bound complexes (Extended Data Fig. 1a). The recently determined crystal structure[10] of a soluble cleaved HIV-1 Env based on the BG505 SOSIP.664 construct was no exception; in particular – while an artificial disulfide and other modifications of the SOSIP.664 construct were critical to production of a homogeneous, soluble, cleaved trimer[17] – antibody PGT122 appeared to facilitate crystallization[10]. Diffraction from crystals of the PGT122 complex, however, extended to only 4.7-Å resolution, hampering the trace of non-helical regions of gp41 as well as the placement and registry of side chains[10]. To obtain improved crystals, we explored the addition of antibody 35O22, which recognizes a gp120-gp41 epitope[13]. Addition of 35O22 to PGT122-bound viral spike in the membrane-bound virion context showed single-molecule fluorescent resonance energy transfer (smFRET) responses that closely resembled those of the mature native unliganded spike (Extended Data Fig. 1b)[18]. In the context of crystallization, addition of 35O22 to the PGT122-BG505 SOSIP.664 complex led to ternary complex crystals in space group $P6_3$. While diffraction was anisotropic, we succeeded in collectin ~3.5 Å data from a single crystal (Extended Data Table 1). Structure solution by molecular replacement with free structures of Fab PGT122[19], Fab 35O22[13] and gp120[20] revealed a double antibody-bound gp120-gp41 protomer to occupy the asymmetric unit and led to an R_{work}/R_{free} of 21.35%/24.80%.

Overall, the HIV-1 spike forms a 3-blade propeller, capped at its membrane-distal apex by antibody PGT122 and at the membrane-proximal end by antibody 35O22 (Fig. 1, Extended Data Fig. 2a,b). Protomer interactions occur through assembled variable regions, V1, V2 and V3, which comprise the trimer association domain[21] at the membrane-distal portion of the spike, and also through gp41, primarily between helical interactions around the trimer axis[10,11]. No trimeric interactions are contributed by the gp120 core; indeed, a cleft or opening is found under the trimer association domains along the 3-fold axis where such associations might occur. Trimeric prefusion gp41 forms a platform through which the gp120 termini extend towards the viral membrane. Unusually slow signal peptide cleavage[6], which keeps the N terminus of gp120 proximal to the membrane, may facilitate folding of prefusion HIV-1 Env.

Prefusion structure of gp41

Prefusion gp41 wraps its hydrophobic core around extended N- and C-termini-strands of gp120 (Fig. 2a). It forms a 4-helix collar comprising helices α6 ($Met530_{gp41}$-$Asn543_{gp41}$), α7 ($Gly572_{gp41}$-$Ile595_{gp41}$), α8 ($Leu619_{gp41}$-$Trp623_{gp41}$), and α9 ($Trp628_{gp41}$-$Asp664_{gp41}$) (the numbering of prefusion gp41 helices and strands continues the nomenclature established for the gp120 subunit, which ends with helix α5 and strand β26; for clarity, the molecule is named after each residue number). The first residue of gp41 visible in electron density corresponds to $Val518_{gp41}$, in the fusion peptide. An extended stretch connects to $Leu523_{gp41}$, which interacts hydrophobically with $Trp45_{gp120}$ and $Ile84_{gp120}$, both of which are part of the 7-stranded β-sandwich around which the gp120-inner domain is organized[22,23]. The main chain of gp41 follows gp120-strand β0 away from the trimer axis towards the viral membrane, until residue $Met530_{gp41}$, where the fold reverses itself and extends through α6 towards the trimer axis and away from the viral membrane. Density between residues 547_{gp41} and 569_{gp41} is sparse (Extended Data Fig. 3a,b), and ultimately connects to helix α7, which forms a parallel coiled-coil about the trimer axis. At the end of α7 is the gp41-cysteine loop (spanned by the $Cys598_{gp41}$-$Cys604_{gp41}$ disulfide), whose C-terminal residues initiate strand β27 ($Leu602_{gp41}$-$Thr606_{gp41}$), which hydrogen bonds in an anti-parallel fashion with strand $\beta\,\bar{4}$ from the N terminus of gp120. The intersubunit disulfide ('SOS')[14] between residues 501_{gp120} and 605_{gp41} welds the C terminus of gp120 to the membrane-proximal end of strand $\beta\,\bar{4}$ (Fig. 2a). Upon passing the gp120 termini, gp41 reaches α8, whose C terminus aligns spatially with the N terminus of α6. After α8, the α9 helix reverses direction, again wrapping past the N and C termini of gp120, before extending horizontally along the edge of the spike to reach the gp120 termini from a neighboring protomer.

Topologically, the gp41 subunit completes a single circle around the gp120 termini with the insertion of a hydrophobic prong comprising the side chain of $Met530_{gp41}$ (which is located at the N terminus of α6, proximal to the fusion peptide), into a triple tryptophan-clasp formed by $Trp623_{gp41}$ (from the C terminus of α8), $Trp628_{gp41}$ (from the N terminus of α9) and $Trp631_{gp41}$ (one turn into α9) (Fig. 2a insert). The alignment of dipoles from helices α6 and α8 likely provides electrostatic complementarity that helps to stabilize the neighboring methionine-tryptophan clasp.

Within a single protomer, the buried surface area between gp41 and gp120 totals 5,270 $Å^2$, including 216 $Å^2$ from glycan-protein interactions (Supplementary Table 1). A substantial portion of this is hydrophobic: gp41 essentially wraps its hydrophobic core around the N and C termini of gp120 (Fig. 2b). Trimer interfaces also bury a large surface area (3,140 $Å^2$ contributed by each protomer, comprising 1,920 $Å^2$ from the gp41-gp41 interface, 861 $Å^2$ from the gp120-gp120 interface and 360 $Å^2$ from the gp120-gp41 interface) (Extended Data Fig. 2c-f). Close to the trimer axis, these involve helix α7, as well as the N-terminal portion of the gp41-cysteine loop. Further from the trimer axis, interactions involve α9. Other than interactions of α7, most interprotomer interactions are hydrophilic (Fig. 2c).

Prefusion to postfusion gp41 transition

To understand the conformational transition from prefusion to postfusion gp41, we compared the gp41-prefusion structure in our antibody-bound HIV-1 Env trimer with previously determined postfusion structures[8,9,24,25] (Fig. 3). Postfusion gp41 comprises two helices, HR1 and HR2 (Fig. 3a); these form a trimeric six-helical bundle, with HR1 helices arranged as an interior parallel coiled-coil, and exterior HR2 helices packing anti-parallel to bring N-terminal fusion peptides and C-terminal transmembrane regions into proximity. Distance difference analysis[26] (Fig. 3b) of prefusion and postfusion structures indicated two regions of structural similarity, corresponding to (i) the prefusion α7 helix aligned with the C-terminal half of the postfusion HR1 helix and (ii) the prefusion α9 helix aligned with much of the postfusion HR2 helix.

Superposition of prefusion α7 and postfusion HR1 placed residues 569_{gp41}-593_{gp41} within 5 Å, with a root-mean-square deviation (rmsd) of 1.35 Å. For this superposition to occur, Cα-movements of over 80 Å are required for the gp41-fusion peptide and α6 helix as well as for the C-terminal portion of the α9 helix. Notably, this superposition preserves the coiled-coil trimeric interactions of both prefusion and postfusion molecules and thus likely mimics the natural conformational transition that occurs during membrane fusion. Meanwhile, superposition of prefusion α9 and postfusion HR2 placed residues 634_{gp41}-664_{gp41} within 5 Å, with an rmsd of 3.58 Å; this substantial alignment of the α9 and HR2 helices indicates that the HR2 helix is mostly preformed in the prefusion structure.

Entry rearrangements of HIV-1 Env

Biosynthesis of HIV-1 Env starts with an uncleaved gp160 trimer. After cleavage, the spike condenses into the prefusion mature closed structure described here. In the gp120-inner domain, helix $\alpha\,\overline{1}$ is formed, and a parallel strand exists between strands β3 and β21; in gp41, we observe helix α7 to begin around residue 571_{gp41}. A partially open EM structure[27] has been reported at 6 Å, in which the trimer association domains appear to be displaced from the trimeric axis, and helical density suggests helix α7 to start several turns earlier; we modeled these rearrangements with a rigid body motion of 6 degrees for gp120 and the conversion of ~15 residues of helix α6 and connecting stretch into helix α7, which extends ~20 Å towards the target cell membrane (Fig. 3d, middle panel; Extended Data Table 2).

The CD4-bound state has been visualized by a number of EM reconstructions[28,29] and atomic-level structures[7,22]. In this state, V1V2 separates from V3: V3 points towards the target cell[30], and the bridging sheet[7] assembles with strand β2 forming antiparallel hydrogen bonds with β21 (as opposed to the parallel β3-β21 interaction of the near-native mature state; notably, the only parallel β-strand in the RSV F glycoprotein prefusion structure also changes conformation in RSV F pre- to postfusion transition[31]). With layer 1 of the inner domain[23], helix α0 forms, and $Gln428_{gp120}$ and strand β21 invert; in layer 2, inner domain rearrangements include the swapping of distinct perpendicular interactions of $Trp112_{gp120}$ and $Trp427_{gp120}$ (Extended Data Fig. 4). CD4 binding allows HR2-peptide analogues (such as C34) to bind[32], and we can model helix α7 starting as early as 554_{gp41} with $Met530_{gp41}$ still in its membrane-proximal tryptophan clasp, as expected because 35O22 binds the CD4-

bound SOSIP.664 (Extended Data Fig. 3d-e, 5c-e). We envision that Env-CCR5 interactions[33] bring the CD4-bound state close to the target cell membrane, where "disassembling α6/assembling α7 helices" coupled to release of the $Met530_{gp41}$ prong from its tryptophan clasp ultimately amasses the gp41-fusion peptide(s) (Fig. 3d, 2nd panel from right, Extended Data Fig. 3f).

At this receptor-bound stage, it is easy to imagine the fusion peptide penetrating the target cell membrane, while strand β27 of the gp41-cysteine loop remains hydrogen bonded to the gp120 termini (and the C terminus of the gp41 ectodomain remains in the viral membrane). Rearrangement of gp41 to its postfusion conformation may be triggered by gp120 shedding[34], with expulsion of the gp120 termini tugging on the gp41-cysteine loop and destabilizing prefusion gp41.

HIV-1 rearrangements and other type I fusion machines

To determine whether the distinct elements we observed in prefusion gp41 were preserved elsewhere, we examined prefusion and postfusion states of other type I fusion machines from influenza virus[35,36] (a member of the Orthomyxoviridae family of viruses), respiratory syncytial virus[31,37] (RSV; Paramyxoviridae), and Ebola virus[38,39] (Filoviridae) (Fig. 4a). In all cases, a helix was observed in the gp41-prefusion equivalents, which corresponds in sequence to the C-terminal portion of the helix that in the postfusion conformation comprises the interior coiled-coil characteristic of type I fusion machines[8,9] (Fig. 4b). With prefusion machines from HIV-1, influenza, and Ebola, the nascent prefusion helix adopts a coiled-coil; with RSV, a coiled-coil assembles immediately N-terminal to the nascent postfusion helix. Despite dramatic differences in gp120-equivalents, similarity is observed in the overall topology of subunit interactions. Notably, all of the gp41-equivalents wrap hydrophobic residues around extended termini (or N terminus) of their gp120-equivalents (Fig. 4c). Overall, the similarities in prefusion folding topology and in prefusion interior helices observed here, along with the previously observed similarity in postfusion coiled-coils (reviewed in [40]), provide a more general and integrated view of the structural and conformational requirements of type I-mediated membrane fusion.

Glycan shield and genetic variation of mature unliganded Env

The prefusion mature closed conformation of HIV-1 Env is the target of most neutralizing antibodies. The newly revealed structure of a near-complete gp120-gp41 Env trimer provides an opportunity to understand aggregate properties of glycosylation and variation. Glycan shielding and genetic variation have long been recognized as mechanisms to avoid antibody recognition[41]. The BG505 SOSIP.664 sequence contains 28 sequons specifying *N*-linked glycosylation (including a T332N mutation). We modeled high mannose glycans (either Man5 or Man9) on each sequon and calculated accessible surface for radii ranging from 1.4 Å (the radius of a water molecule) to 10 Å (the approximate radius of a single immunoglobulin domain) (Extended Data Fig. 6). In the Man9-glycosylated model, 29% of the protein surface was solvent accessible, whereas only 3% of the surface was immunoglobulin-domain accessible. By contrast, with the fusion glycoproteins from

influenza and RSV, 14% and 48%, respectively, of these surfaces were immunoglobulin-domain accessible (Fig. 5a).

In terms of genetic variation, we calculated the per-residue Shannon entropy of 3,943 sequences of HIV-1 (Fig. 5b). Approximately 50% of the surface was shown to have a variability of greater than 10%, a degree of surface variation shared by influenza, but not by RSV. When we combined glycan shielding and genetic variation, only ~2% of the surface was immunoglobulin accessible with a variability of less than 10% (Extended Data Fig. 7, upper panels); much of this conserved surface occurred at the membrane-proximal "base" of the spike, which is expected to be sterically occluded by the viral membrane. To determine how this fully assembled shield compared to other conformations, we also assessed the immunoglobulin accessibility of the CD4-bound conformation (Extended Data Fig. 7, lower panels). Notably, the CD4-bound conformation showed substantially higher levels of glycan-free, conserved surface, consistent with the greater ease by which antibodies reactive with the CD4-bound conformation are elicited – and by contrast, the difficulty in eliciting broadly neutralizing antibodies against the glycan-covered, sequence-variable prefusion closed state.

Serologic recognition of mature Env

Despite multiple mechanisms of immune evasion that shield mature HIV-1 Env, potent broadly neutralizing antibodies do develop[42]. The structure of HIV-1 Env in the prefusion mature closed state allows us to map known epitopes on their most likely functional target (Fig. 6a) and to compare the recognition of broadly neutralizing HIV-1 antibodies, with those capable of neutralizing influenza virus and RSV (Fig. 6b).

To determine the location and prevalence of effective humoral responses, we used a serologic analysis based on serum neutralization of a panel of diverse HIV-1 isolates[20]. Sera from a cohort that had been infected for 2-3 years and from another that had been infected for more than 5 years were assessed on a panel of 21 diverse HIV-1 isolates, and the neutralization phenotypes assigned to 12 prototypic antibody-neutralization fingerprints (Fig. 6c, Extended Data Fig. 8a,b). We then mapped the responses to the surface of the mature closed HIV-1-Env spike (Extended Data Fig. 8c,d). The most prevalent response corresponded to the glycan-V3 epitope epitomized by antibody PGT128. CD4-binding site-directed responses, 8ANC195 responses, and V1V2-directed responses were prevalent. Overall, responses in both cohorts were highly correlated indicating little evolution in the location or prevalence of effective neutralizing responses between 2-3 and 5+ years. Notably, when mapping Env sites of vulnerability, the majority of prevalent sites corresponded to Env surfaces covered by *N*-linked glycosylation and/or of high sequence variability. Indeed, both PGT122 and 35O22 co-crystallized here recognize *N*-linked glycan, and they both utilize framework 3 insertions, in the light chain for PGT122 and in the heavy chain for 35O22 (Extended Data Fig. 9).

Viral evasion and immune recognition

In addition to merging virus and host-cell membranes, viral fusion machines must contend with antibody-mediated neutralization. With RSV, peak infection occurs at 5-10 months of

life, as maternal antibodies wane; with influenza virus, natural infection elicits strain-specific antibodies, and evasion occurs seasonally on a global scale. HIV-1, however, confronts the immune system in each individual directly, often presenting high titer of Env antigens over years of chronic infection. These differences in evasion are reflected by structural difference in the fusion machines. The structure of the HIV-1-Env spike revealed here allows the molecular trickery behind single spike entry[43], glycan shielding[3], and conformational masking[44] to be visualized at the atomic level (Extended Data Fig. 10). Thus, avoidance of antibody avidity[45] through the ability of a single HIV-1 spike to fuse viral and target cell membranes[43] is likely assisted by membrane-proximity of the co-receptor and membrane-association of the MPER (Fig. 3); despite these differences, the HIV-1-Env spike appears to share mechanism and topology with other type I fusion machines (Fig. 4). In terms of glycan shielding[3], we have modeled the structure of a fully assembled glycan shield for BG505, a tier II-transmitted founder virus[46] (Fig. 5). While glycan masking appears complete at the HIV-1-spike apex, closer to the viral membrane "holes" in the glycan shield are observed. And with conformational masking[44], evasion is optimal for the prefusion mature closed state, with CD4-binding unmasking conserved glycan-free surfaces (Extended Data Fig. 7). Despite extraordinary glycosylation and sequence variation, the human immune system appears up to the challenge of generating HIV-1-neutralizing antibodies (Fig. 6). We note that recognition of glycosylation appears to be a trait common only to HIV-1-neutralizing antibodies and that both broadly neutralizing HIV-1 and influenza virus antibodies tolerate epitope-sequence variation (Fig. 6b). The structure of the HIV-1-Env spike described here thus reveals not only commonalities in entry and evasion with other type I fusion machines, but also commonalities in recognition by the human immune system. It remains to be seen whether an effective vaccine against HIV-1 can be developed by using the atomic-level detail provided here, which should allow for immunogen-design strategies such as conformational stabilization[47] and nanoparticle delivery[48]; additionally, antibody-type and ontogeny-specific strategies may be required, and template ontogenies are becoming available for some of the more commonly elicited HIV-1-neutralizing antibodies (Extended Data Fig. 8d), such as those against the CD4-binding site[49] and V1V2 sites[50].

Methods

BG505 SOSIP.664 expression and purification

The crystallized HIV-1-Env construct from strain BG505 was generated following published reports[10,15,16], using BG505 genbank accession numbers ABA61516 and DQ208458[46]; including the "SOS" mutations (A501C, T605C), the isoleucine to proline mutation at residue 559 (I559P), and the glycan site at residue 332 (T332N); mutating the cleavage site to 6R (REKR to RRRRRR); and truncating the C terminus to residue 664 (all HIV-1 Env numbering according to the HX nomenclature). This construct is referred to as BG505 SOSIP.664 throughout this entire manuscript.

The BG505 SOSIP.664 construct was co-transfected with furin in HEK 293 GnTI−/− cells using 600 μg of BG505 SOSIP.664 and 150 μg of furin plasmid DNAs as described previously[16]. Transfection supernatants were harvested after 7 days, and passed over either a

2G12 antibody- or VRC01 antibody-affinity column. After washing with phosphate-buffered saline (PBS), bound proteins were eluted with 3M $MgCl_2$, 10 mM Tris pH 8.0. The eluate was concentrated to less than 5 ml with Centricon-70 and applied to a Superdex 200 column, equilibrated in 5 mM HEPES, pH 7.5, 150 mM NaCl, 0.02% azide. The peak corresponding to trimeric HIV-1 Env was identified, pooled, concentrated and used immediately or flash-frozen in liquid nitrogen and stored at −80° C.

Fab expression and purification

PGT122 and 35O22 IgGs were expressed as previously described[51]. Heavy chain plasmids containing an HRV3C cleavage site in the hinge region were co-transfected with light chain plasmids in 293F (35O22) or GnTI−/− (PGT122, which is glycosylated) using TrueFect-Max transfection reagent (United Biosystems) according to manufacturer's protocol. Cultures were fed with fresh 293FreeStyle media (Life Technologies) 4 h post-transfection and with HyClone SFM4HEK293 enriched medium (HyClone) containing valproic acid (4 mM final concentration) 24 h after transfection. Cultures were then incubated at 33° C for 6 days, and supernatants harvested and passed over a protein A affinity column. After PBS wash and low pH elution, pH of eluate was neutralized with 1M Tris pH 8.5. Fabs were obtained using HRV3C digestion and collecting flow-thru from protein A column to remove Fc fraction. Fabs were further purified over Superdex 200 in 5 mM HEPES, pH 7.5, 150 mM NaCl, 0.02% azide.

Ternary complex preparation

PGT122 and 35O22 Fabs were added to a solution of purified trimeric BG505 SOSIP.664 in 5-fold molar excess for 30 min at room temperature (RT). The complex was then partially deglycosylated by adding Endo H (50 μl) for 1 hour at RT in the gel filtration buffer. The complex was then purified over gel filtration equilibrated in 5mM HEPES, pH 7.5, 150 mM NaCl, 0.02% azide. Fractions were pooled, concentrated down to 5-10 OD_{280}/mL and used immediately for crystal screening or flash frozen in liquid nitrogen and kept at −80° C until further use.

Crystallization screening

The ternary complex was screened for crystallization using 572 conditions from Hampton, Wizard and Precipitant Synergy[52] screens using a Cartesian Honeybee crystallization robot as described previously[51] and a mosquito robot using 0.1 μl of reservoir solution and 0.1 μl of protein solution. Crystals suitable for structural determination were identified robotically in 0.2M Li_2SO_4, 6.65% PEG 1500, 20% isopropanol and 0.1M sodium acetate pH 5.5. Crystals were reproduced in hanging droplets containing 0.5 μl of reservoir solution and 0.5 μl of protein solution. Optimal crystallization conditions were obtained in 16% isopropanol, 5.32% PEG 1500, 0.2M Li_2SO_4, 0.1M Na acetate pH 5.5. Crystals were cryoprotected in a solution of 15% 2R3R-butanediol, 5% isopropanol, 0.2M Li_2SO_4, 6.65% PEG 1500, 0.1M sodium acetate pH 5.5, and flash-frozen after covering with paratone N[53]. Data were collected at a wavelength of 1.00 Å at the SER-CAT beamline ID-22 (Advanced Photon Source, Argonne National Laboratory).

X-ray data collection, structure solution and model building

Diffraction data were processed with the HKL2000 suite[54]. The data were corrected for anisotropy using the anisotropy server http://services.mbi.ucla.edu/anisoscale/ with truncations to 3.5 Å, 3.5 Å, 3.1 Å along a, b, and c axes, respectively. Structure solution was obtained with Phaser using gp120 (PDB ID: 4J6R[20]), PGT122 (PDB ID: 4JY5[19]) and 35O22 Fv (PDB ID: 4TOY[13]) as search models. Refinement was carried out with Phenix[55] imposing PGT122, 35O22 and gp120 model-based refinement restraint during initial round of refinement. Model building was carried out with Coot[56]. The Ramachandran plot as determined by MOLPROBITY[57] showed 92.66% of all residues in favored regions and 99.03% of all residues in allowed regions. Data collection and refinement statistics are shown in Extended Data Table 1.

Preparation of fluorescently labeled virus

For site-specific incorporation of fluorophores the Q3 (GQQQLG) and A1 (GDSLDMLEWSLM) peptides were inserted into the V1 and V4 loops of HIV-1 JR-FL gp160 at positions 136 and 404 (HXB2 numbering), respectively. Virus for smFRET imaging was generated by cotransfecting HEK293 cells with a 40:1 ratio of wild-type HIV-1 JR-FL gp160 plasmid pCAGGS to HIV-1 JR-FL gp160 plasmid containing the Q3 and A1 labelling peptides, in addition to pNL4-3 Δenv ΔRT. The virus was harvested 24 h post-transfection, concentrated by centrifugation, and fluorescently labelled with donor and acceptor fluorophores through incubation with 0.5 μM Cy3B-cadaverine, 0.5 μM Cy5(4S)COT-CoA, 0.65 μM transglutaminase[58] (Sigma), and 5 μM AcpS (REF to PMID 17465518) overnight at room temperature. The AcpS enzyme and the CoA-conjugated fluorophore were prepared as described[59]. DSPE-$PEG_{2,000}$-biotin (Avanti) was then added to the reaction at a final concentration of 6 μM (0.02 mg/ml), and the labelled virus was purified by ultracentrifugation for 1 h at 150,000 × g over a 6-18% Optiprep (Sigma) gradient.

smFRET data acquisition and analysis

Fluorescently labeled virions were immobilized on streptavidin-coated quartz microscope slides and imaged on a prism-based total internal reflection fluorescence microscope. The donor fluorophore was excited by a 532-nm laser (Laser Quantum). The donor and acceptor fluorescence emissions were collected through a 60-X water objective (Nikon), split by a 650DCXR dichroic filter (Chroma), and focused on parallel EMCCD cameras (Photometrics). Movies were recorded at 25 frames/s for 40 s. smFRET imaging was performed in buffer containing 50 mM Tris pH7.5, 100 mM NaCl, a cocktail of triplet-state quenchers[60], and 2 mM protocatechuic acid and 8 nM protocatechuate 3,4-deoxygenase to remove molecular oxygen[61]. Where indicated, surface-bound viruses were incubated with 0.1 mg/ml PGT122 and/or 0.1 mg/ml 35O22 antibody.

All data analysis was performed using custom written Matlab software. Fluorescence trajectories were extracted from the movies, and used to calculate FRET efficiency according to FRET = IA/(ID+IA). smFRET trajectories were identified for analysis on basis of their displaying sufficient signal-to-noise and fluorophore lifetime. FRET trajectories were compiled into histograms, which were fit to the sum of three Gaussian distributions in

Matlab. smFRET revealed that the HIV-1 Env is conformationally dynamic, transitioning between three distinct conformational states. Response to various ligands identified the low-FRET state as the closed unliganded conformation of HIV-1 Env and the intermediate- and high-FRET states as the activated conformations stabilized by coreceptor and CD4 binding, respectively.

Binding studies using biolayer interferometry

A fortéBio Octet Red384 instrument was used to measure binding of BG505 SOSIP. 664 and BG505 gp120 molecules to a panel of antibodies (VRC01, VRC03, b6, b12, F105, PGT122, PGT128, PGT135, 2G12, 8ANC195, 17b, 2.2C, 412d, 48D, 447-52D, PG9, PG16, PGT145, VRC26.09, 35O22, PGT151) and CD4 Ig. All the assays were performed with agitation set to 1,000 rpm in PBS buffer supplemented with 1% bovine serum albumin (BSA) in order to minimize nonspecific interactions. The final volume for all the solutions was 40-50 μl/well. Assays were performed at 30°C in solid black tilted-bottom 384-well plates (Geiger Bio-One). Human antibodies (40-50 μg/ml) in PBS buffer was used to load anti-human IgG Fc capture (AHC) probes for 600 s. Typical capture levels were between 1 and 1.5 nm, and variability within a row of eight tips did not exceed 0.1 nm. Biosensor tips were then equilibrated for 180 s in PBS/1% BSA buffer prior to binding assessment of the BG505 SOSIP.664 and BG505 gp120 molecules in solution for 300 s; binding was then allowed to dissociate for 300s. Parallel correction to subtract systematic baseline drift was carried out by subtracting the measurements recorded for a sensor without monoclonal antibody incubated in PBS/1% BSA. Data analyses were carried out using Octet software, version 8.0.

Difference distance analysis

Difference distance matrices[26] were produced by distance sorting atom positions and plotting with the program DDMP[62].

Surface plasmon resonance analysis

Affinities and kinetics of binding of antibodies 35O22 and PGT151 to BG505 SOSIP.664 soluble trimer were assessed by surface plasmon resonance on a Biacore T-200 (GE Healthcare) at 20° C with buffer HBS-EP+ (10 mM HEPES, pH 7.4, 150 mM NaCl, 3 mM EDTA, and 0.05% surfactant P-20). In general, mouse anti-human Fc antibody was first immobilized onto two flow cells on a CM5 chip at ~10,000 response units (RU) with standard amine coupling protocol (GE Healthcare). Either CD4-Ig, 2G12 IgG or 17b IgG was then captured on both flow cells by flowing over a 200 nM solution at 5 μl/min flow rate for two minutes. This was followed by a 1-minute injection of 1 μM human Fc on both flow cells to block unliganded mouse anti-human Fc antibody. The captured 2G12, CD4 or 17b were used to immobilize BG505 SOSIP.664 trimer on only one flow cell, with no trimer captured on the other flow cell (reference cell). For capturing with 2G12 or CD4-Ig, 500 nM of unliganded trimer was used, whereas, a complex of 500 nM trimer + 1500 nM sCD4 was used for capturing with 17b. Antibody Fab fragments at 2-fold dilutions starting from 885 nM, 600 nM and 460 nM for 35O22, PGT151 and PGT145, respectively, were injected over the captured trimer channel and the reference channel at a flow rate of 50 μl/min for 2 minutes and allowed to dissociate for 3-30 minutes depending on the rate of dissociation of

each interaction. The cells were regenerated with two 10 μl injections of 3.0 M $MgCl_2$ at a flow rate of 100 μl/min. Blank sensorgrams were obtained by injection of same volume of HBS-EP+ buffer in place of antibody Fab fragments. Sensorgrams of the concentration series were corrected with corresponding blank curves and fitted globally with Biacore T200 evaluation software using a 1:1 Langmuir model of binding. The stoichiometry of binding of antibodies to the trimer were estimated by normalizing the R_{max} values to the amount of trimer captured and performing linear regression analysis using the R_{max} values for the antibodies with known stoichiometries.

Modeling of missing loops, side chains, and the *N*-linked glycan shield

Missing loops not defined in the HIV-1-Env trimer crystal structure were modeled using Loopy[63]. Missing side chains were modeled with Scap[64].

To model the *N*-linked glycan shield, we first determined all possible *N*-linked sequons in the HIV-1 Env trimer structure. A single asparagine residue in each sequon was targeted for computational *N*-linked glycan addition using a series of oligomannose 9 rotamer libraries at different resolutions. In constructing the rotamer libraries, the asparagine side chain rotamers were also considered. To avoid a combinatorial explosion in the search space, select torsion angles in the oligomannose 9 rotamer libraries were allowed to vary in increments between 30-60 degrees. We used an overlap factor (*ofac*) to screen for clashes between the sugar moieties and the trimer structure. The *ofac* between two nonbonded atoms is defined as the distance between two atoms divided by the sum of their van der Waal's radii. For the modeling carried out here, we set the *ofac* to a value of 0.60. For sterically occluded positions, the *ofac* was set to 0.55. To remove steric bumps between sugar moieties, all models were subjected to 100 cycles of conjugate gradient energy minimization using the GLYCAM[65] force field in Amber12[66] with a distance-dependent dielectric.

Mapping sequence variability onto trimer structure

For each of HIV-1 Env, influenza HA, and RSV F, residue sequence variability was computed as the Shannon entropy for each residue position, based on representative sets of 3943 HIV-1 strains, 4467 influenza strains, and 212 RSV strains, respectively. Residues were colored based on the computed entropy values, on a scale of white (conserved) to purple (variable).

Chronically infected cohort information

In the CHAVI 001 cohort, high-risk subjects were screened for HIV-1 infection by ELISA, Western blotting, and plasma RNA to recruit individuals with acute HIV infection, who were then followed for ~2 years until plasma neutralization breadth developed[67]. In addition, a group of individuals were enrolled in the CHAVI 001 or CHAVI 008 cohorts who were chronically infected with HIV-1 strains clade A, B or C, and were screened for plasma neutralization breadth. The trial participants were enrolled at sites in Tanzania, South Africa, Malawi, the United States, and the United Kingdom[68]. Both CHAVI001 and CHAVI008 protocols were approved by the institutional review boards of each of the participating institutions where blood samples were received or processed for analysis, and informed consent was obtained from all subjects.

Serum neutralization fingerprinting analysis

The prevalence of effective neutralizing responses against HIV-1 Env in cohorts from 2-3 and 5+ years post-infection was estimated using a neutralization fingerprinting approach, as described previously[20]. Briefly, serum neutralization over a set of 21 diverse viral strains was compared to neutralization of the same viruses by a set of broadly neutralizing antibodies grouped into 12 epitope-specific antibody clusters. For each serum, the relative prevalence of each of the 12 antibody specificities was estimated by representing serum neutralization as a linear combination of the monoclonal specificities, with prevalence values of 0.2 deemed as positive. Sera with less than 30% breadth on the 21-virus panel as well as sera with high residual values from the computation (data not shown) were not included in the analysis. For mapping prevalence values onto the BG505 SOSIP.664 structure, residues part of multiple antibody epitopes were colored according to the respective antibody specificity with the highest prevalence in the 5+ years cohort. Antibody neutralization was measured using single-round-of-infection HIV-1 Env-pseudoviruses and TZM-bl target cells, as described previously[69]. Neutralization curves were fit by nonlinear regression using a 5-parameter hill slope equation as previously described[69].

Epitope analysis for HIV-1 Env, influenza HA, and RSV F antibodies

Glycan usage and average residue entropy were calculated for seven representative HIV-1 Env (VRC01, b12, CD4, 8ANC195, PG9, PGT122, 2G12, and 35O22)[7,51,70-73], four representative influenza HA (2D1, C05, F10, and CR8043)[74-77], and three representative RSV F (D25, Motavizumab, and 101F)[31,78,79] epitopes based on their respective crystal structures. The selection of the flu antibodies was done as follows: F10 (stem targeting) and C05 (head targeting) were selected based on their cross-neutralizing ability for group 1 and group 2 of influenza A. CR8043 (group 2 specific) and 2D1 (H1 specific), which target distinct regions from F10 and C05 at the stem and head of the HA respectively, were also selected for epitope analysis. An antigen residue was defined as an epitope residue if it had a non-zero BSA in the crystal structure. The fraction of glycan surface area in an epitope was calculated as the buried surface area of epitope glycans divided by the buried surface area of the full epitope. Unpaired nonparametric Mann-Whitney test[80] was used to quantify the statistical difference between glycan fraction or average residue entropy for HIV-1 versus influenza or RSV antibody epitopes.

Extended Data

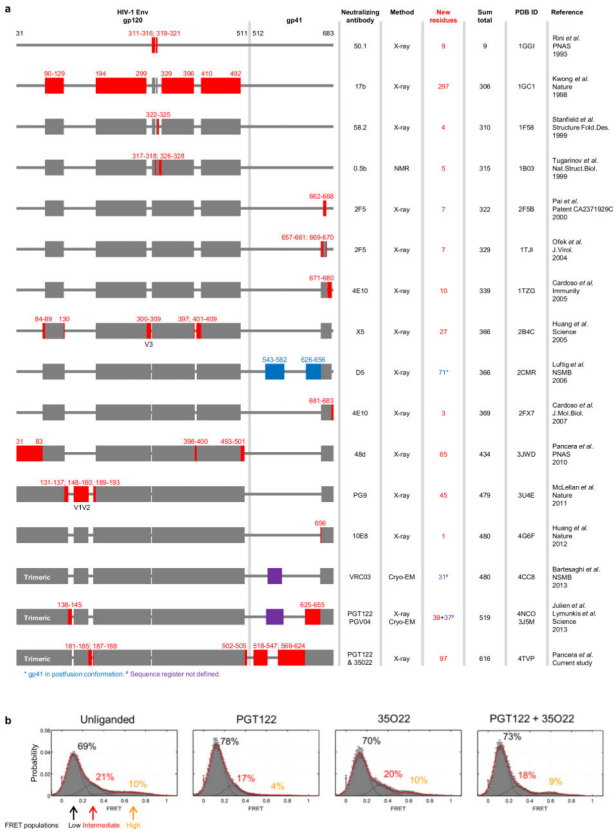

Extended Data Figure 1. Antibody-mediated crystallization and antibody-induced conformation

a, Atomic-level structures for HIV-1-Env regions determined in complex with HIV-1-neutralizing antibodies. Neutralizing antibodies generally recognize the prefusion conformation of HIV-1 Env. Structures highlighted here display a cumulative sum total of prefusion HIV-1-Env structural information. Env residues are numbered according to standard HX numbering (from PDBs). One structure, for antibody D5 (blue), is in the postfusion gp41 conformation, and is not included in the sum total. Regions of other structures (purple), did not define sequence register, and were also not included in the sum total. Reference listed here are cited elsewhere in the manuscript, except for Rini et al., 1993[87], Stanfield et al., 1999[88,89], Ofek et al., 2004[90], Cardoso et al., 2005[91], Luftig et al., 2006[92], Cardoso et al., 2007[93]. **b**, Antibody-induced conformation of HIV-1 Env in the context of infectious JR-FL virions as assessed by smFRET. HIV-1_{JR-FL} gp160 was labelled with fluorescent dyes in variable regions, V1 and V4, at positions that did not interfere with Env function (see methods), and virus was surface immobilized for imaging via total internal reflection fluorescence microscopy[18]. smFRET trajectories were compiled into histograms for the HIV-1_{JR-FL} Env trimer, either unliganded or after pre-incubation for 30 min with 0.1 mg/ml PGT122, 35O22, or both PGT122 and 35O22 prior to imaging. Resultant Env conformational landscapes could be deconvoluted into three gaussian distributions: a low-FRET population that predominated for the prefusion mature unliganded state, and intermediate- and high-FRET populations, which predominated in the presence of

CD4 receptor and CD4-induced antibody[18]. smFRET trajectories are shown for the unliganded HIV-1_{JR-FL} Env trimer as well as in the presence of PGT122, 35O22, and both PGT122 and 35O22. The concordance between conformational ensembles indicates unliganded and PGT122+35O22-bound conformation to be similar (Spearman correlation coefficient of 0.988). Interestingly, the presence of just one of the antibodies (PGT122) appeared to reduce the high FRET population, an effect not observed in the presence of both antibodies; this suggests that the antibody-induced stability of a particular state is not solely additive, and that antibodies can both induce a particular conformational state as well as alter the transition dynamics from that state.

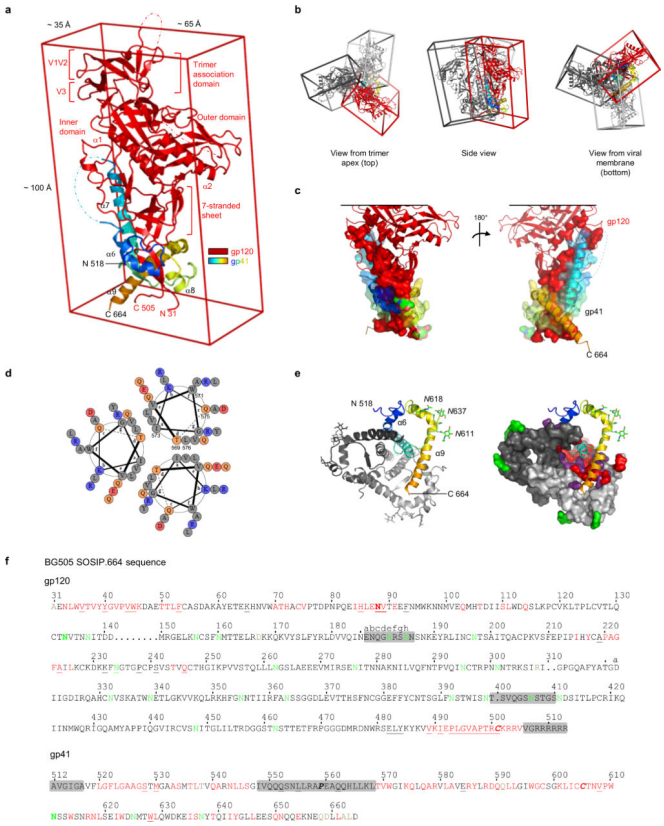

Extended Data Figure 2. HIV-1 subunit interactions: principle component analysis and interface contacts

a, Minimum-bounding box, generated by principle component analysis, encasing 90% of the HIV-1-Env gp120-gp41 protomer. Each gp120-gp41 blade forms a rectangle of height of ~100 Å, width of ~65 Å, and thickness of ~35 Å. Subunits are displayed in ribbon representation with gp41 colored rainbow and gp120 colored and labeled red. As previously visualized[10,11], the membrane-distal portion of the rectangle is made up of the gp120-outer and -inner domains, with the central 7-stranded β-sandwich of the inner domain occupying the trimer-distal, membrane-proximal portion of gp120. We have now resolved the rest of the spike: the membrane-proximal portion of the rectangle is made up of gp41, with the membrane-distal portion of gp41 closest to the molecular 3-fold axis occupied by helix α7 (which corresponds in register to the C-terminal portion of the postfusion HR1 helix of gp41), and the rest of gp41 folding around N- and C-termini-strands of gp120, which extend

over 20 Å toward the viral membrane. **b**, Different views of trimeric protomer association. The protomer association at the membrane-distal trimer apex occurs through the corners of the minimum-bounding box, whereas the association at the membrane-proximal region occurs with substantial interpenetration of the minimum-bounding box; these interaction differences and the protruding nature of the gp120 outer domain result in the overall mushroom shape of the trimer. **c**, gp120-gp41 interface. Ribbon representation of gp120 (red) and gp41 (rainbow from blue N terminus to orange C terminus), with gp120 residues that interact with gp41 shown in surface representation and gp41 residues that interact with gp120 shown in semitransparent surface. A complete list of subunits interactions is provided in Supplementary Table 1. Membrane-proximal interactions are further stabilized by hydrophobic interactions, which gp41 makes with the N and C termini of gp120 –such as between $Trp35_{gp120}$ and $Pro609_{gp41}$ and between $Trp610_{gp41}$ and $Pro498_{gp120}$. **d**, Wheel diagram representation of α7 coiled-coil in the prefusion mature closed conformation of gp41 as generated by DrawCoil 1.0: http://www.grigoryanlab.org/drawcoil/[94]. **e**, gp41-trimer interfaces as viewed from the viral membrane in ribbon and surface representation (90° rotation from Fig. 2c). **f**, BG505 SOSIP.664 sequence with residues identified by mutagenesis[95-101] to be important for gp120/gp41 association underlined. Residues that were found to interact between gp120 and gp41 by examination of the crystal structure are indicated in red (intra-protomer interactions) and in brown (inter-protomer interactions). Sites of *N*-linked glycosylation are shown in green; glycan N88 is shown in red because it is part of the gp120/gp41 interactions; no density was observed for potential *N*-linked glycans at residues 185, 398, 406, 411, 462 and 625. Residues that were disordered in the crystal structure are gray. SOS (A501C/T605C) and IP (I559P) mutations are labeled in bold and italics. Dots indicate residues not present in the BG505 sequence.

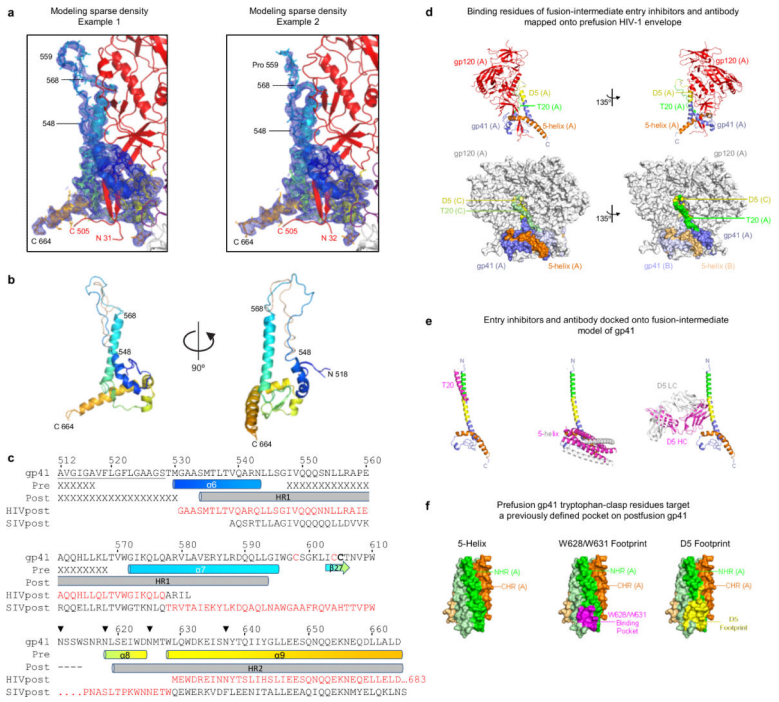

Extended Data Figure 3. Modeling of gp41: prefusion α6-to-α7 density, HIV-1/SIV postfusion chimera, and liganded interactions

a, Modeling of gp41 residues 548-568. At low contour, suggestive density is observed that might correspond to the connection between α6 and α7 helices. To investigate the degree to which a model for this region might be defined, we built and refined two different models for this region: electron density (blue) shown for $2F_0$-F_c density at 1σ contour; gp41 (rainbow color from blue to orange) shown in ribbon representation with side chains; gp120 (red) shown in ribbon representation. The location of the I559P mutation is indicated. **b**, The two models from panel **a** are superimposed and shown in perpendicular orientations. **c**, HIV-1-SIV postfusion chimera. Sequences of HIV-1 gp41 from prefusion structure (BG505 strain, PDB ID: 4TVP), postfusion structure (HIVpost, PDB ID: 2X7R[24]) and SIV gp41 postfusion structure (SIVpost, PDB ID: 2EZO[25]) are aligned with secondary structure indicated. Residues that were used to make the postfusion HIV-1/SIV chimera used in Figure 3 are highlighted in red. **d**, Binding residues of representative fusion-intermediate entry inhibitors or antibodies mapped onto the structure of prefusion HIV-1-Env spike[102-104]. (top) Ribbon representation of prefusion envelope protomer A (gp120 in red and gp41 in blue) at two orientations, with the binding residues of the fusion-intermediate inhibitors 5-helix,T20, and of monoclonal antibody D5[92] shown in orange, green, and yellow, respectively. (bottom) Surface representation of the prefusion envelope trimer, with inhibitor and antibody binding residues mapped onto the surfaces of all protomers. gp120 is colored gray and gp41 is colored in shades of blue, depending on protomer. Binding residues of fusion-intermediate inhibitors 5-helix, T20, and monoclonal antibody D5 are shown in same color shades as in the top panels. **e.** 5-helix, T20 and D5 Fab (all colored magenta and gray) docked onto a model of fusion-intermediate gp41 (colored as in **d**). **f**, A previously defined binding pocket on postfusion gp41 is the target of prefusion gp41 tryptophan-clasp residues Trp628 and Trp631. Shown is a surface representation of gp41 5-helix protein[104] (left, with N-heptad repeat (NHR) helices colored in shades of green and C-heptad repeat (CHR) helices colored in shades of orange). The footprint of gp41 tryptophan-clasp residues Trp628 and Trp631 is shown in magenta (middle) and that of a representative NHR-specific neutralizing antibody, D5, in yellow [92,105,106] (right).

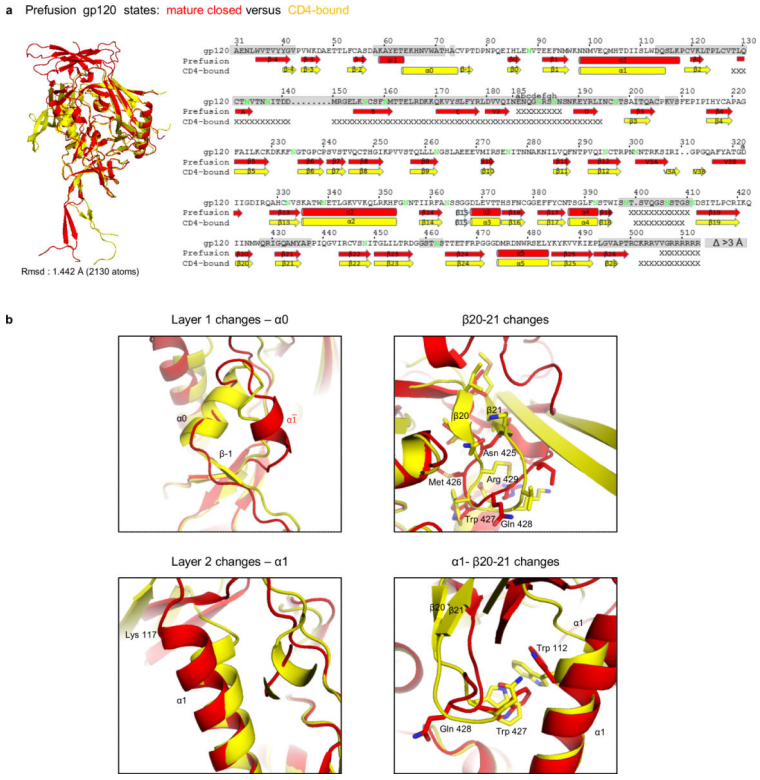

Extended Data Figure 4. Conformational changes between prefusion mature closed state and CD4-bound state of gp120

a, Overall structure and sequence comparison. gp120 is shown in ribbon representation in prefusion mature closed (red) and CD4-bound (yellow, PDB ID: 3JWD[22]) conformation. V1V2 (PDB ID: 3U2S[51]) has been modeled onto the CD4-bound conformation. Secondary structure is defined for prefusion and CD4-bound conformation on the BG505 sequence, with cylinders representing α-helix and arrows β-strands. Disordered residues are indicated by "X". Residues that move more than 3 Å between the mature closed and the CD4-bound gp120 conformations are shown with grey shadows. Sites of *N*-linked glycosylation are shown in green. **b**. Details of conformational changes between the mature closed (red) and the CD4-bound conformations (yellow) of gp120 (shown in ribbon): regions highlighted cover layer 1 with changes at α0 (we note that density in this region is not well defined), layer 2 with changes at α1 and β20-21 rearrangements. All atoms rmsd are: residues 54-74$_{gp120}$, rmsd = 4.759 Å; residues 98-117 $_{gp120}$, rmsd = 0.497 Å; 424-436 $_{gp120}$, rmsd = 3.196 Å.

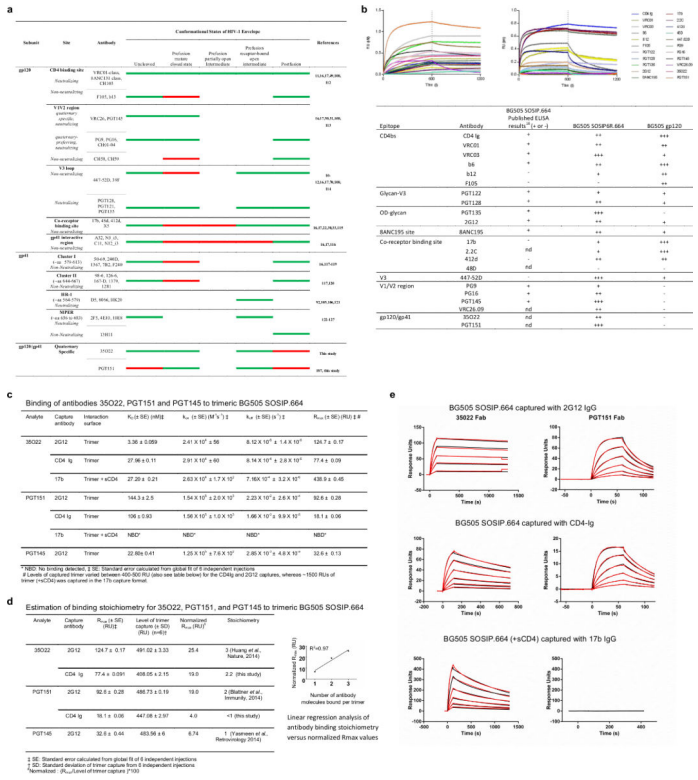

Extended Data Figure 5. Antigenic profiles of HIV-1 envelope conformational states

a, Qualitative recognition of HIV-1 envelope by diverse antibodies is shown for five conformational states. Green bars indicate reported recognition, red bars no recognition, and absence of a bar indicates that recognition is undefined. The compiled data is from both cited references and experiments described in this figure. **b**, Octet Biosensorgrams of BG505 SOSIP.664 (left) and BG505 gp120 (right) binding to human monoclonal IgGs. The dotted line indicates the beginning of the dissociation phase and the maximal specific binding after 300 s reported in the table (− <0.05 RU, + 0.05 RU to 0.25 RU, ++ 0.25 RU to 0.5 RU, and +++ >0.5 RU). BG505gp120 did not contain the T332N mutation (no glycan at that position). Both proteins were made in GnTi−/−. We note that antigenicity of the BG505 SOSIP.664 and BG505gp120 protein varied depending on the assay done. Thus, using surface plasmon resonance, no CD4i antibodies binding was detected while some binding could be observed using biolayer interferometry. Although PG9 bound BG505gp120 in ELISA[16], it did not bind in biolayer interferometry format. We observed 447-52D binding while it was not observed in ELISA[16]. **c**, SPR binding affinities of 35O22, PGT151 and PGT145 to BG505 SOSIP.664 and influence of sCD4. **d**, Estimation of binding stoichiometry for 35O22, PGT151, and PGT145 to trimeric BG505 SOSIP.664 by SPR and comparison to published data[13,107,108]. **e**, Effect of sCD4 and sCD4/17b on binding of antibodies 35O22 and PGT151 to BG505 SOSIP.664 by SPR. The structure of a prefusion mature closed state of HIV-1 provides a critical addition to the pantheon of HIV-1 Env structures with atomic-level detail. Moreover, antibodies 35O22 and PGT151, which bind specifically to the trimeric prefusion conformation of gp41, provide new tools by which to assess the conformational state of gp41[13,107,109]. The binding of antibodies 35O22 and PGT151 to BG505 SOSIP.664 trimer was tested in the presence of the CD4 receptor and the

17b antibody[110] (a co-receptor surrogate which recognizes a bridging sheet epitope that overlaps the site of co-receptor recognition). In the case of antibody 35O22, CD4 binding to the BG505 SOSIP.664 trimer impacted the kinetics, affinity and stoichiometry of binding. 35O22 bound to BG505 SOSIP.664 with an 8.4-fold reduced affinity, primarily contributed by an increased rate of dissociation. The overall binding level (R_{max}) normalized to the average level of trimer captured (see also panel **d**) was lower suggesting substoichiometric binding. Capturing the trimer on a CD4-Ig surface reduced normalized R_{max} for PGT151 compared to the 2G12 capture format, suggesting reduced stoichiometry for PGT151 binding to trimer pre-bound with CD4, although kinetics and affinity of interaction were similar. A BG505 SOSIP.664 trimer + sCD4 complex captured onto a 17b surface bound 35O22 but showed no detectable binding to PGT151.

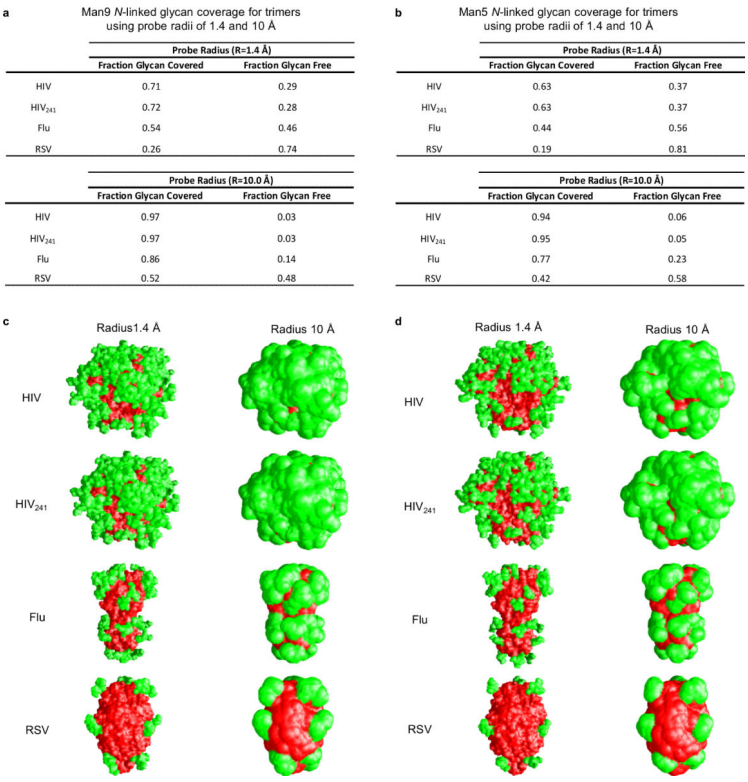

Extended Data Figure 6. *N*-Linked glycan occlusion of type I fusion machines

The prefusion mature closed conformation of HIV-1 Env evades the humoral immune response with a fully assembled glycan shield. Here we calculate and display the solvent-accessible surface of glycan and protein for HIV-1 Env, influenza virus hemagglutinin and RSV fusion glycoprotein. Calculations of the percentage coverage of the protein surface were determined for trimeric type I fusion machines based on two probe sizes of 1.4 Å (solvent radius) and 10.0 Å (the estimated steric footprint of an antibody combining region). Surface area calculations were carried out according to Kong et. al[79], and images were generated using Grasp v1.3[80]. All models were refined using Amber with the GLYCAM force field (see Methods for details). The PDB IDs associated with the glycosylated models are: 4TVP (HIV-1), 2YP7[85] (Flu) and 4JHW[31] (RSV). The strains associated with the PDB IDs are: BG505.SOSIP.664 (HIV-1), H3N2 A/Hong Kong/4443/2005 (Flu) and A/A2/61

(RSV). The solvent-accessible protein surface is shown in red, and *N*-linked glycans are shown in green. **a**, Estimated Man9 glycan coverage. **b**, Estimated Man5 glycan coverage. **c**, Visualization of Man9 *N*-linked glycan coverage for two probe radii. **d**, Visualization of Man5 *N*-linked glycan coverage for two probe radii.

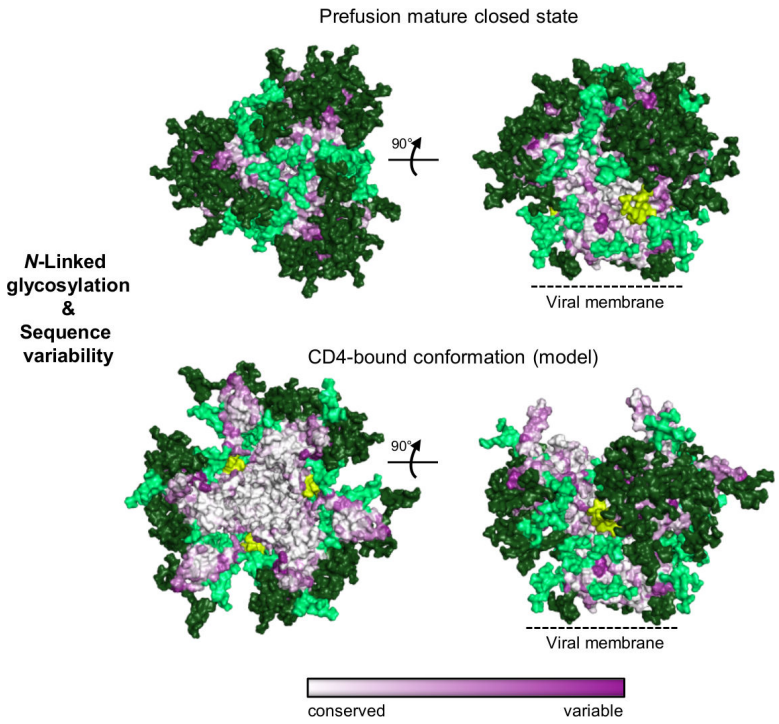

Extended Data Figure 7. Glycan shield and sequence variability for HIV-1 prefusion mature closed and CD4-bound conformations

Many conformations of HIV-1 Env divert the immune response. Thus for example, shed gp120 and post-fusion gp41 represent dominant viral antigens; however these forms of Env are not functional, and antibodies that only target them are not neutralizing. Functional conformations, however, may be significantly shielded from the neutralizing antibody. The CD4-bound conformation of HIV-1 Env, for example, is only functionally present when the viral and target-cell membranes are in close proximity, and the exposed co-receptor binding site (including V3- and CD4-induced epitopes) is spatially occluded from neutralizing antibody. Here we provide models for the prefusion closed state versus the CD4-bound conformation, which display the fully assembled glycan shield and surface Env variability. Env *N*-linked glycans are depicted in light green (conserved; greater than 90% conservation) or dark green (variable; less than 90% conservation) on the mature closed Env structure and modeled CD4-bound conformation. Env sequence variability is shown from white to purple (conserved to variable). A conserved glycan at residue 241_{gp120} not present in the BG505 sequence is shown in yellow-green. As can be seen, the prefusion closed state has few glycan-free surfaces, whereas the CD4-bound state exposes substantial glycan-free conserved surface.

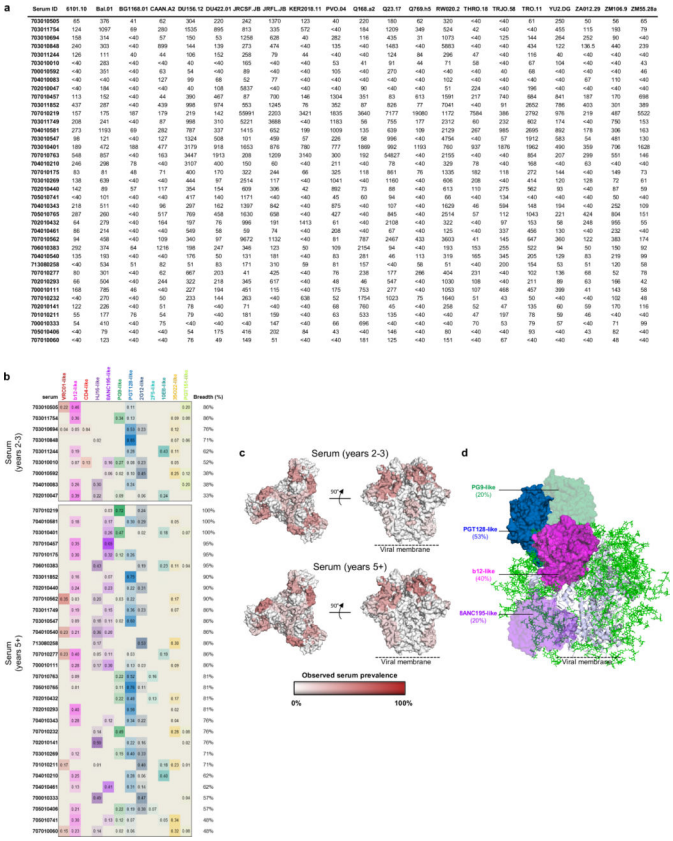

Extended Data Figure 8. Prevalence of neutralizing responses identified serologically from cohorts from 2-3 years and 5+ years post infection

a, Serum neutralization on 21-strain virus panel. ID_{50}s are shown for serum (rows) titrated against HIV-1 viral strains (columns). **b**, For each serum, the predicted neutralization prevalence for each of 12 antibody specificities is shown based on neutralization of 21 diverse HIV-1 strains. **c**, Prevalence of antibody specificities onto the HIV-1-Env colored as indicated in the bar graph. **d**, The antibody specificities for high serum prevalence in the 5+ years cohort are depicted by Fabs of representative antibodies (surface transparency proportional to prevalence) binding the BG505 SOSIP.664 Env trimer, shown in grey ribbon representation, with glycans as green sticks. Note that while prevalence is highly correlated, there were notable differences, for example between PGT151 at 2-3 years and 5+ years in this study, as well as between the cohorts analyzed here and in ref. 13.

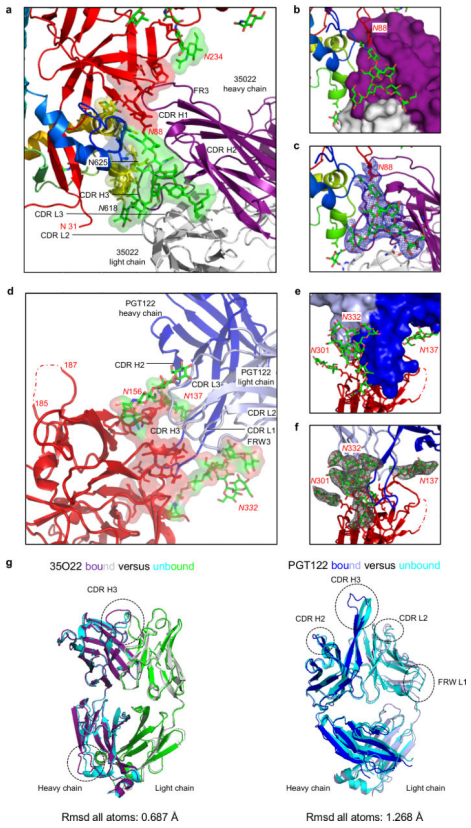

Extended Data Figure 9. Antibodies 35O22 and PGT122: interface with HIV-1 Env and comparison of bound and unbound Fab conformations

Despite the substantial immune evasion protecting the mature unliganded state from humoral recognition, after several years of infection, the human immune system does generate broadly neutralizing antibodies. 35O22 and PGT122 are two of these antibodies, which neutralize 62% and 65% of HIV-1 isolates at a median IC_{50} of 0.033 and 0.05 μg/ml, respectively[13, 12]. Here we provide additional details on 35O22 and PGT122 recognition. **a**, 35O22 Fab is shown in ribbon representation (purple (heavy chain) and white (light chain)). The gp120 subunit is shown in red, the gp41 subunit in rainbow (from blue N terminus to orange C terminus), and glycans in green sticks. Complementary determining regions (CDRs) are labeled, and interactive HIV-1-Env residues highlighted in semi-transparent surface representation. At the membrane-distal surface of 35O22, an extended framework 3 region (FW3) of the heavy chain (resulting from an insertion of 8 residues) interacts with strand β1 of the 7-stranded inner domain sandwich of gp120. The heavy chain-CDRs form extensive contacts with the *N*-linked glycan extending from residue 88_{gp120}. In addition to glycan contacts, the CDR H3 of 35O22 interacts with the α9 helix of gp41. Helix α9 interactions are also made by the FW3 of the light chain (a complete list of contacts is provided in Supplementary Table 3). Overall, 35O22 buries 1,105 $Å^2$ solvent surface on gp120 (including 793 $Å^2$ with the $Asn88_{gp120}$ glycan) and 594 $Å^2$ solvent surface on gp41 (including 127 $Å^2$ with the $Asn618_{gp41}$ glycan). Despite residue 625_{gp41} being part of the glycan sequon “NMT”, no glycan is observed; indeed, the side-chain amide of residue 625_{gp41} hydrogen bonds with the side-chain oxygen of Tyr32 in the 35O22 heavy chain, and the presence of an *N*-linked glycan at residue 625_{gp41} is difficult to reconcile with 35O22

recognition. **b**, Same colors as **a**, with 35O22 Fab shown in surface representation. **c**, Same colors as **a**, with $2F_o$-F_c at 1σ contour (blue density) shown around glycan 88 of gp120. Antibody 35O22 employs a novel mechanism of glycan-protein recognition, combining a protruding FW3 with CDR H1, H2 and H3 to form a "bowl" that holds glycan. FW3 and CDR H3 provide the top edges of the bowl and interact with the protein surface of gp120, whereas CDR H1 and H2 are recessed and hold/recognize glycan. This structural mechanism of recognition contrasts with the extended CDR H3-draping glycan observed with other antibodies that penetrate the glycan shield such as PG9[51] and PGT128[78]. **d**, PGT122 interface details. Ribbon representation of PGT122 Fab in blue (heavy chain) and light blue (light chain) interacting with one gp120 subunit shown in red with glycans in green sticks. Complementary determining regions (CDRs) are labeled, and interactive HIV-1-Env residues highlighted in surface representation. Primary contacts between antibody PGT122 and *N*-linked glycan involve *N*137 and *N*332, with minor contact with *N*156. Although portions of glycan *N*301 can be observed in the electron density, no direct contacts with PGT122 are observed; a complete list of contacts between PGT122 and BG505 SOSIP.664 is provided in Supplementary Table 4. **e**, Same colors as **d**, with PGT122 Fab shown in surface representation, **f**, Same colors as **d**, with $2F_o$-F_c at 1σ contour (grey density) shown around glycan 332 of gp120. **g**,Comparison of bound and unbound Fab conformations. Unbound and HIV-1-Env bound Fabs were superimposed, and ribbon representations and rmsds are displayed. (Left) Unbound 35O22 Fab is colored cyan (heavy chain) and green (light chain) and bound 35O22 Fab deep purple (heavy chain) and white (light chain). (Right) Unbound PGT122 Fab is colored cyan, and bound PGT122 Fab blue (heavy chain) and light blue (light chain). Regions which showed conformational changes are highlighted with black dotted lines. We note that in the 35O22 bound conformation, density is poor and/or sparse for the Fc portion of the Fab.

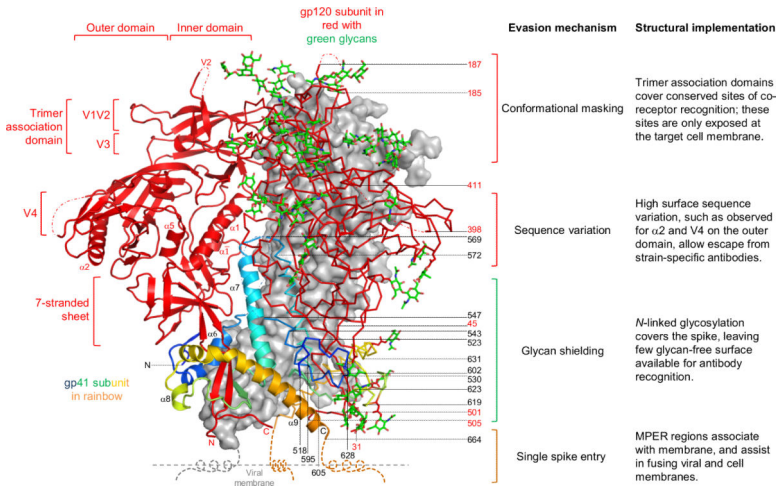

Extended Data Figure 10. Structural implementation of HIV-1 molecular trickery

The prefusion HIV-1-Env trimer (left) is displayed with evasion mechanisms and their structural implementation (right). The gp120 subunit is shown in red, the gp41 subunit in rainbow (from blue N terminus to orange C terminus), and crystallographically defined glycans in green. One protomer is shown with Cα trace and glycans in stick representation, a

second protomer is shown in ribbon representation with secondary structure elements labeled, and the third protomer is shown in light grey surface. The MPER region for each protomer is shown as a stylized helix associated with the viral membrane. The location of secondary structural elements, termini, and residues called in the text has been labeled (red font for gp120 and black font for gp41).

Extended Data Table 1 Data collection and refinement statistics.

	BG505 SOSIP.664 with PGT122 and 35022
Data collection	
Space group	$P6_3$
Cell dimensions	
a, *b*, *c* (Å)	128.89, 128.89, 313.42
a, *β*, *γ* (°)	90.0, 90.0, 120.0
Resolution (Å)	50-3.10 (3.68-3.49, 3.49-3.34, 3.34-3.21, 3.21-3.10)*
R_{sym} or R_{merge}	11.6 (44.9, 52.7, 68.3, 75.5)
$I/\sigma I$	11.3 (2.22, 1.95, 1.43, 1.11)
Completeness (%)	73.4 (57.2, 40.6, 33.9, 27.8)
Redundancy	3.8 (3.3, 3.4, 3.3, 3.0)
Refinement	
Resolution (Å)	40.739-3.098 (3.4893-3.3375; 3.3375-3.2091; 3.2091-3.0984)
No. reflections	29,353
R_{work}/R_{free}	0.2135/0.2480 (0.3056/0.3484; 0.3348/0.3315; 0.4039/0.4056)
No. atoms	12189
Protein	11345
Ligand (glycans)	757
Sulfate ion	50
Water	37
B-factors (Å^2)	109.50
Protein	109.30
Ligand (glycans)	113.34
Sulfate ion	140.95
Water	40.20
R.m.s deviations	
Bond lengths (Å)	0.002
Bond angles (°)	0.575
Ramachadran Favored %	92.66
Ramachadran Allowed %	99.03

	BG505 SOSIP.664 with PGT122 and 35022
MolProbity all-atoms clashscore	5.36
MolProbity score	1.80
PDB ID	4TVP

Extended Data Table 2

Modeling parameters for gp120 and gp41 rearrangements.

	Prefusion mature closed state	Prefusion partially open intermediate	Prefusion receptor-bound open intermediate	Postfusion
gp120	**Crystal structure (4TVP)**	**Crystal structure (4TVP)**	**Crystal structure of core (3JWD) with modeled V3 (3HI1) and V1V2 (3U4E)**	**Crystal structure of core (3JWD) with modeled V3 (3HI1) and V1V2 (3U4E)**
V1V2	Native	Rotated 6°	Rotated to align with bridging sheet	Rotated to align with bridging sheet
V3	Native	Rotated 6°	Protruding towards target cell	Protruding towards target cell
Core	Native	Rotated 6°	Rotated 50°	Rotated 50°
N+C-term	Native	Native	Unknown	Rotated 45°

gp41	**Crystal structure (4TVP)**	**Crystal structure (4TVP) with modeled α7**	**Crystal structure (4TVP) with modeled α7 and α6 removed**	**Crystal structure (chimera of 2X7R and 2EZO)**
α6	Native	Disassembling to α7	Disassembled	Extended to postfusion HR1
α7	Native	Extending	Extended with fusion peptide	Extended to postfusion HR1
α8	Native	Native	Native	Extended to postfusion HR2
α9	Native	Native	Native	Extended to postfusion HR2

Supplementary Material

Refer to Web version on PubMed Central for supplementary material.

Acknowledgments

We thank colleagues that contributed reagents, carried out clinical protocols, and provided discussions and comments on the manuscript, as detailed in supplementary information. Support for this work was provided by the Intramural Research Program of the Vaccine Research Center, National Institute of Allergy and Infectious Diseases (NIAID), National Institutes of Health, and by grants from the National Institutes of Health, from the Irvington Fellows Program of the Cancer Research Program, and from the International AIDS Vaccine Initiative's (IAVI's) Neutralizing Antibody Consortium. Use of sector 22 (Southeast Region Collaborative Access Team) at the Advanced Photon Source was supported by the US Department of Energy, Basic Energy Sciences, Office of Science, under contract number W-31-109-Eng-38.

References

1. The Joint United Nations Programme on HIV/AIDS. 2013 Report on the global AIDS epidemic. 2013
2. Wyatt R, Sodroski J. The HIV-1 envelope glycoproteins: fusogens, antigens, and immunogens. Science. 1998; 280:1884–1888. [PubMed: 9632381]
3. Wei X, et al. Antibody neutralization and escape by HIV-1. Nature. 2003; 422:307–312. [PubMed: 12646921]
4. Leonard CK, et al. Assignment of intrachain disulfide bonds and characterization of potential glycosylation sites of the type 1 recombinant human immunodeficiency virus envelope glycoprotein (gp120) expressed in Chinese hamster ovary cells. The Journal of biological chemistry. 1990; 265:10373–10382. [PubMed: 2355006]
5. Cimbro R, et al. Tyrosine sulfation in the second variable loop (V2) of HIV-1 gp120 stabilizes V2-V3 interaction and modulates neutralization sensitivity. Proceedings of the National Academy of Sciences of the United States of America. 2014; 111:3152–3157. [PubMed: 24569807]
6. Li Y, et al. Effects of inefficient cleavage of the signal sequence of HIV-1 gp 120 on its association with calnexin, folding, and intracellular transport. Proceedings of the National Academy of Sciences of the United States of America. 1996; 93:9606–9611. [PubMed: 8790377]
7. Kwong PD, et al. Structure of an HIV gp120 envelope glycoprotein in complex with the CD4 receptor and a neutralizing human antibody. Nature. 1998; 393:648–659. [PubMed: 9641677]
8. Chan DC, Fass D, Berger JM, Kim PS. Core structure of gp41 from the HIV envelope glycoprotein. Cell. 1997; 89:263–273. [PubMed: 9108481]
9. Weissenhorn W, Dessen A, Harrison SC, Skehel JJ, Wiley DC. Atomic structure of the ectodomain from HIV-1 gp41. Nature. 1997; 387:426–430. [PubMed: 9163431]
10. Julien JP, et al. Crystal structure of a soluble cleaved HIV-1 envelope trimer. Science. 2013; 342:1477–1483. [PubMed: 24179159]
11. Lyumkis D, et al. Cryo-EM structure of a fully glycosylated soluble cleaved HIV-1 envelope trimer. Science. 2013; 342:1484–1490. [PubMed: 24179160]
12. Walker LM, et al. Broad neutralization coverage of HIV by multiple highly potent antibodies. Nature. 2011; 477:466–470. [PubMed: 21849977]
13. Huang J, et al. Broad and potent neutralization of HIV-1 by a human antibody that recognizes an intersubunit site on the envelope glycoprotein. Nature. 2014 In Press.
14. Sanders RW, et al. Stabilization of the soluble, cleaved, trimeric form of the envelope glycoprotein complex of human immunodeficiency virus type 1. Journal of virology. 2002; 76:8875–8889. [PubMed: 12163607]
15. Julien JP, et al. Asymmetric recognition of the HIV-1 trimer by broadly neutralizing antibody PG9. Proceedings of the National Academy of Sciences of the United States of America. 2013; 110:4351–4356. [PubMed: 23426631]

16. Sanders RW, et al. A next-generation cleaved, soluble HIV-1 Env Trimer, BG505 SOSIP.664 gp140, expresses multiple epitopes for broadly neutralizing but not non-neutralizing antibodies. PLoS pathogens. 2013; 9:e1003618. [PubMed: 24068931]
17. Ringe RP, et al. Cleavage strongly influences whether soluble HIV-1 envelope glycoprotein trimers adopt a native-like conformation. Proceedings of the National Academy of Sciences of the United States of America. 2013; 110:18256–18261. [PubMed: 24145402]
18. Munro JB, et al. Conformational dynamics of HIV Env molecules on the surface of native virions. Biophys J. 2013; 104:415A.
19. Julien JP, et al. Broadly neutralizing antibody PGT121 allosterically modulates CD4 binding via recognition of the HIV-1 gp120 V3 base and multiple surrounding glycans. PLoS pathogens. 2013; 9:e1003342. [PubMed: 23658524]
20. Georgiev IS, et al. Delineating antibody recognition in polyclonal sera from patterns of HIV-1 isolate neutralization. Science. 2013; 340:751–756. [PubMed: 23661761]
21. Mao Y, et al. Subunit organization of the membrane-bound HIV-1 envelope glycoprotein trimer. Nature structural & molecular biology. 2012; 19:893–899.
22. Pancera M, et al. Structure of HIV-1 gp120 with gp41-interactive region reveals layered envelope architecture and basis of conformational mobility. Proceedings of the National Academy of Sciences of the United States of America. 2010; 107:1166–1171. [PubMed: 20080564]
23. Finzi A, et al. Topological layers in the HIV-1 gp120 inner domain regulate gp41 interaction and CD4-triggered conformational transitions. Molecular cell. 2010; 37:656–667. [PubMed: 20227370]
24. Buzon V, et al. Crystal structure of HIV-1 gp41 including both fusion peptide and membrane proximal external regions. PLoS pathogens. 2010; 6:e1000880. [PubMed: 20463810]
25. Caffrey M, et al. Three-dimensional solution structure of the 44 kDa ectodomain of SIV gp41. The EMBO journal. 1998; 17:4572–4584. [PubMed: 9707417]
26. Nishikawa K, Ooi T, Saito N, Isogai Y. Tertiary Structure of Proteins .1. Representation and Computation of Conformations. Journal of the Physical Society of Japan. 1972; 32:1331–1337.
27. Bartesaghi A, Merk A, Borgnia MJ, Milne JL, Subramaniam S. Prefusion structure of trimeric HIV-1 envelope glycoprotein determined by cryo-electron microscopy. Nature structural & molecular biology. 2013; 20:1352–1357.
28. Liu J, Bartesaghi A, Borgnia MJ, Sapiro G, Subramaniam S. Molecular architecture of native HIV-1 gp120 trimers. Nature. 2008; 455:109–113. [PubMed: 18668044]
29. White TA, et al. Molecular architectures of trimeric SIV and HIV-1 envelope glycoproteins on intact viruses: strain-dependent variation in quaternary structure. PLoS pathogens. 2010; 6:e1001249. [PubMed: 21203482]
30. Huang CC, et al. Structure of a V3-containing HIV-1 gp120 core. Science. 2005; 310:1025–1028. [PubMed: 16284180]
31. McLellan JS, et al. Structure of RSV fusion glycoprotein trimer bound to a prefusion-specific neutralizing antibody. Science. 2013; 340:1113–1117. [PubMed: 23618766]
32. Yuan W, Craig S, Si Z, Farzan M, Sodroski J. CD4-induced T-20 binding to human immunodeficiency virus type 1 gp120 blocks interaction with the CXCR4 coreceptor. Journal of virology. 2004; 78:5448–5457. [PubMed: 15113923]
33. Huang CC, et al. Structures of the CCR5 N terminus and of a tyrosine-sulfated antibody with HIV-1 gp120 and CD4. Science. 2007; 317:1930–1934. [PubMed: 17901336]
34. Moore JP, McKeating JA, Weiss RA, Sattentau QJ. Dissociation of gp120 from HIV-1 virions induced by soluble CD4. Science. 1990; 250:1139–1142. [PubMed: 2251501]
35. Wilson IA, Skehel JJ, Wiley DC. Structure of the haemagglutinin membrane glycoprotein of influenza virus at 3 A resolution. Nature. 1981; 289:366–373. [PubMed: 7464906]
36. Bullough PA, Hughson FM, Skehel JJ, Wiley DC. Structure of influenza haemagglutinin at the pH of membrane fusion. Nature. 1994; 371:37–43. [PubMed: 8072525]
37. McLellan JS, Yang Y, Graham BS, Kwong PD. Structure of respiratory syncytial virus fusion glycoprotein in the postfusion conformation reveals preservation of neutralizing epitopes. Journal of virology. 2011; 85:7788–7796. [PubMed: 21613394]

38. Weissenhorn W, Carfi A, Lee KH, Skehel JJ, Wiley DC. Crystal structure of the Ebola virus membrane fusion subunit, GP2, from the envelope glycoprotein ectodomain. Molecular cell. 1998; 2:605–616. [PubMed: 9844633]
39. Lee JE, et al. Structure of the Ebola virus glycoprotein bound to an antibody from a human survivor. Nature. 2008; 454:177–182. [PubMed: 18615077]
40. Colman PM, Lawrence MC. The structural biology of type I viral membrane fusion. Nature reviews. Molecular cell biology. 2003; 4:309–319. [PubMed: 12671653]
41. Wyatt R, et al. The antigenic structure of the HIV gp120 envelope glycoprotein. Nature. 1998; 393:705–711. [PubMed: 9641684]
42. Hraber P, et al. Prevalence of broadly neutralizing antibody responses during chronic HIV-1 infection. AIDS. 2014; 28:163–169. [PubMed: 24361678]
43. Yang X, Kurteva S, Ren X, Lee S, Sodroski J. Stoichiometry of envelope glycoprotein trimers in the entry of human immunodeficiency virus type 1. Journal of virology. 2005; 79:12132–12147. [PubMed: 16160141]
44. Kwong PD, et al. HIV-1 evades antibody-mediated neutralization through conformational masking of receptor-binding sites. Nature. 2002; 420:678–682. [PubMed: 12478295]
45. Klein JS, Bjorkman PJ. Few and far between: how HIV may be evading antibody avidity. PLoS pathogens. 2010; 6:e1000908. [PubMed: 20523901]
46. Wu X, et al. Neutralization escape variants of human immunodeficiency virus type 1 are transmitted from mother to infant. Journal of virology. 2006; 80:835–844. [PubMed: 16378985]
47. McLellan JS, et al. Structure-based design of a fusion glycoprotein vaccine for respiratory syncytial virus. Science. 2013; 342:592–598. [PubMed: 24179220]
48. Kanekiyo M, et al. Self-assembling influenza nanoparticle vaccines elicit broadly neutralizing H1N1 antibodies. Nature. 2013; 499:102–106. [PubMed: 23698367]
49. Liao H-X, et al. Co-evolution of a broadly neutralizing HIV-1 antibody and founder virus. Nature. 2013; 496:469–476. [PubMed: 23552890]
50. Doria-Rose NA, et al. Developmental pathway for potent V1V2-directed HIV-neutralizing antibodies. Nature. 2014; 509:55–62. [PubMed: 24590074]
51. McLellan JS, et al. Structure of HIV-1 gp120 V1/V2 domain with broadly neutralizing antibody PG9. Nature. 2011; 480:336–343. [PubMed: 22113616]
52. Majeed S, et al. Enhancing protein crystallization through precipitant synergy. Structure. 2003; 11:1061–1070. [PubMed: 12962625]
53. Kwong PD, Liu Y. Use of cryoprotectants in combination with immiscible oils for flash cooling macromolecular crystals. Journal of Applied Crystallography. 1999; 32:102–105.
54. Otwinowski Z, Minor W. Processing of X-ray diffraction data collected in oscillation mode. Methods Enzymol. 1997; 276:307–326.
55. Adams PD, et al. Recent developments in the PHENIX software for automated crystallographic structure determination. J Synchrotron Radiat. 2004; 11:53–55. [PubMed: 14646133]
56. Emsley P, Cowtan K. Coot: model-building tools for molecular graphics. Acta crystallographica. Section D, Biological crystallography. 2004; 60:2126–2132.
57. Davis IW, Murray LW, Richardson JS, Richardson DC. MOLPROBITY: structure validation and all-atom contact analysis for nucleic acids and their complexes. Nucleic Acids Res. 2004; 32:W615–619. [PubMed: 15215462]
58. Lin CW, Ting AY. Transglutaminase-catalyzed site-specific conjugation of small-molecule probes to proteins in vitro and on the surface of living cells. Journal of the American Chemical Society. 2006; 128:4542–4543. [PubMed: 16594669]
59. Zhou Z, et al. Genetically encoded short peptide tags for orthogonal protein labeling by Sfp and AcpS phosphopantetheinyl transferases. ACS chemical biology. 2007; 2:337–346. [PubMed: 17465518]
60. Dave R, Terry DS, Munro JB, Blanchard SC. Mitigating unwanted photophysical processes for improved single-molecule fluorescence imaging. Biophys J. 2009; 96:2371–2381. [PubMed: 19289062]

61. Aitken CE, Marshall RA, Puglisi JD. An oxygen scavenging system for improvement of dye stability in single-molecule fluorescence experiments. Biophys J. 2008; 94:1826–1835. [PubMed: 17921203]
62. Richards FM, Kundrot CE. Identification of structural motifs from protein coordinate data: secondary structure and first-level supersecondary structure. Proteins. 1988; 3:71–84. [PubMed: 3399495]
63. Xiang Z, Soto CS, Honig B. Evaluating conformational free energies: the colony energy and its application to the problem of loop prediction. Proceedings of the National Academy of Sciences of the United States of America. 2002; 99:7432–7437. [PubMed: 12032300]
64. Xiang Z, Honig B. Extending the accuracy limits of prediction for side-chain conformations. Journal of molecular biology. 2001; 311:421–430. [PubMed: 11478870]
65. Kirschner KN, et al. GLYCAM06: a generalizable biomolecular force field. Carbohydrates. Journal of computational chemistry. 2008; 29:622–655. [PubMed: 17849372]
66. Cornell WD, C. P, Bayly CI, Gould IR, Merz KM, Ferguson DM, Spellmeyer DC, Fox T, Caldwell JW, Kollman PA. A Second Generation Force Field for the Simulation of Proteins, Nucleic Acids, and Organic Molecules. J. Am. Chem. Soc. 1995; 117:5179–5197.
67. Tomaras GD, et al. Initial B-cell responses to transmitted human immunodeficiency virus type 1: virion-binding immunoglobulin M (IgM) and IgG antibodies followed by plasma anti-gp41 antibodies with ineffective control of initial viremia. Journal of virology. 2008; 82:12449–12463. [PubMed: 18842730]
68. Tomaras GD, et al. Polyclonal B Cell Responses to Conserved Neutralization Epitopes in a Subset of HIV-1-Infected Individuals. Journal of virology. 2011; 85:11502–11519. [PubMed: 21849452]
69. Li M, et al. Human Immunodeficiency Virus Type 1 env Clones from Acute and Early Subtype B Infections for Standardized Assessments of Vaccine-Elicited Neutralizing Antibodies. Journal of virology. 2005; 79:10108–10125. [PubMed: 16051804]
70. Zhou T, et al. Structural Basis for Broad and Potent Neutralization of HIV-1 by Antibody VRC01. Science. 2010; 329:811–817. [PubMed: 20616231]
71. Zhou T, et al. Structural definition of a conserved neutralization epitope on HIV-1 gp120. Nature. 2007; 445:732–737. [PubMed: 17301785]
72. Scharf L, et al. Antibody 8ANC195 Reveals a Site of Broad Vulnerability on the HIV-1 Envelope Spike. Cell reports. 2014; 7:785–795. [PubMed: 24767986]
73. Calarese DA, et al. Antibody domain exchange is an immunological solution to carbohydrate cluster recognition. Science. 2003; 300:2065–2071. [PubMed: 12829775]
74. Xu R, et al. Structural basis of preexisting immunity to the 2009 H1N1 pandemic influenza virus. Science. 2010; 328:357–360. [PubMed: 20339031]
75. Ekiert DC, et al. Cross-neutralization of influenza A viruses mediated by a single antibody loop. Nature. 2012; 489:526–532. [PubMed: 22982990]
76. Sui J, et al. Structural and functional bases for broad-spectrum neutralization of avian and human influenza A viruses. Nature structural & molecular biology. 2009; 16:265–273.
77. Friesen RH, et al. A common solution to group 2 influenza virus neutralization. Proceedings of the National Academy of Sciences of the United States of America. 2014; 111:445–450. [PubMed: 24335589]
78. McLellan JS, et al. Structural basis of respiratory syncytial virus neutralization by motavizumab. Nature structural & molecular biology. 2010; 17:248–250.
79. McLellan JS, et al. Structure of a major antigenic site on the respiratory syncytial virus fusion glycoprotein in complex with neutralizing antibody 101F. Journal of virology. 2010; 84:12236–12244. [PubMed: 20881049]
80. Mann HBW, Donald R. “On a Test of Whether one of Two Random Variables is Stochastically Larger than the Other”. Annals of Mathematical Statistics. 1947; 18:50.
81. The PyMOL Molecular Graphics System. DeLano Scientific; San Carlos, CA: 2002.
82. Weis WI, Brunger AT, Skehel JJ, Wiley DC. Refinement of the influenza virus hemagglutinin by simulated annealing. Journal of molecular biology. 1990; 212:737–761. [PubMed: 2329580]

83. Chen J, Skehel JJ, Wiley DC. N- and C-terminal residues combine in the fusion-pH influenza hemagglutinin HA(2) subunit to form an N cap that terminates the triple-stranded coiled coil. Proceedings of the National Academy of Sciences of the United States of America. 1999; 96:8967–8972. [PubMed: 10430879]
84. Malashkevich VN, et al. Core structure of the envelope glycoprotein GP2 from Ebola virus at 1.9-A resolution. Proceedings of the National Academy of Sciences of the United States of America. 1999; 96:2662–2667. [PubMed: 10077567]
85. Lin YP, et al. Evolution of the receptor binding properties of the influenza A(H3N2) hemagglutinin. Proceedings of the National Academy of Sciences of the United States of America. 2012; 109:21474–21479. [PubMed: 23236176]
86. Chen L, et al. Structural basis of immune evasion at the site of CD4 attachment on HIV-1 gp120. Science. 2009; 326:1123–1127. [PubMed: 19965434]
87. Rini JM, et al. Crystal structure of a human immunodeficiency virus type 1 neutralizing antibody, 50.1, in complex with its V3 loop peptide antigen. Proceedings of the National Academy of Sciences of the United States of America. 1993; 90:6325–6329. [PubMed: 8327513]
88. Stanfield R, et al. Dual conformations for the HIV-1 gp120 V3 loop in complexes with different neutralizing fabs. Structure. 1999; 7:131–142. [PubMed: 10368281]
89. Tugarinov V, Zvi A, Levy R, Anglister J. A cis proline turn linking two beta-hairpin strands in the solution structure of an antibody-bound HIV-1IIIB V3 peptide. Nat Struct Biol. 1999; 6:331–335. [PubMed: 10201400]
90. Ofek G, et al. Structure and mechanistic analysis of the anti-human immunodeficiency virus type 1 antibody 2F5 in complex with its gp41 epitope. Journal of virology. 2004; 78:10724–10737. [PubMed: 15367639]
91. Cardoso RM, et al. Broadly neutralizing anti-HIV antibody 4E10 recognizes a helical conformation of a highly conserved fusion-associated motif in gp41. Immunity. 2005; 22:163–173. [PubMed: 15723805]
92. Luftig MA, et al. Structural basis for HIV-1 neutralization by a gp41 fusion intermediate-directed antibody. Nature structural & molecular biology. 2006; 13:740–747.
93. Cardoso RM, et al. Structural basis of enhanced binding of extended and helically constrained peptide epitopes of the broadly neutralizing HIV-1 antibody 4E10. Journal of molecular biology. 2007; 365:1533–1544. [PubMed: 17125793]
94. Grigoryan G, Keating AE. Structural specificity in coiled-coil interactions. Current opinion in structural biology. 2008; 18:477–483. [PubMed: 18555680]
95. Helseth E, Olshevsky U, Furman C, Sodroski J. Human immunodeficiency virus type 1 gp120 envelope glycoprotein regions important for association with the gp41 transmembrane glycoprotein. Journal of virology. 1991; 65:2119–2123. [PubMed: 2002555]
96. Thali M, Furman C, Helseth E, Repke H, Sodroski J. Lack of correlation between soluble CD4-induced shedding of the human immunodeficiency virus type 1 exterior envelope glycoprotein and subsequent membrane fusion events. Journal of virology. 1992; 66:5516–5524. [PubMed: 1501286]
97. Cao J, et al. Effects of amino acid changes in the extracellular domain of the human immunodeficiency virus type 1 gp41 envelope glycoprotein. Journal of virology. 1993; 67:2747–2755. [PubMed: 8474172]
98. Leavitt M, Park EJ, Sidorov IA, Dimitrov DS, Quinnan GV Jr. Concordant modulation of neutralization resistance and high infectivity of the primary human immunodeficiency virus type 1 MN strain and definition of a potential gp41 binding site in gp120. Journal of virology. 2003; 77:560–570. [PubMed: 12477860]
99. Yang X, Mahony E, Holm GH, Kassa A, Sodroski J. Role of the gp120 inner domain beta-sandwich in the interaction between the human immunodeficiency virus envelope glycoprotein subunits. Virology. 2003; 313:117–125. [PubMed: 12951026]
100. Sen J, Jacobs A, Caffrey M. Role of the HIV gp120 conserved domain 5 in processing and viral entry. Biochemistry. 2008; 47:7788–7795. [PubMed: 18597484]
101. Wang J, Sen J, Rong L, Caffrey M. Role of the HIV gp120 conserved domain 1 in processing and viral entry. The Journal of biological chemistry. 2008; 283:32644–32649. [PubMed: 18815131]

102. Lawless MK, et al. HIV-1 membrane fusion mechanism: structural studies of the interactions between biologically-active peptides from gp41. Biochemistry. 1996; 35:13697–13708. [PubMed: 8885850]
103. Chen CH, Matthews TJ, McDanal CB, Bolognesi DP, Greenberg ML. A molecular clasp in the human immunodeficiency virus (HIV) type 1 TM protein determines the anti-HIV activity of gp41 derivatives: implication for viral fusion. Journal of virology. 1995; 69:3771–3777. [PubMed: 7538176]
104. Root MJ, Kay MS, Kim PS. Protein design of an HIV-1 entry inhibitor. Science. 2001; 291:884–888. [PubMed: 11229405]
105. Gustchina E, et al. Structural basis of HIV-1 neutralization by affinity matured Fabs directed against the internal trimeric coiled-coil of gp41. PLoS pathogens. 2010; 6:e1001182. [PubMed: 21085615]
106. Sabin C, et al. Crystal structure and size-dependent neutralization properties of HK20, a human monoclonal antibody binding to the highly conserved heptad repeat 1 of gp41. PLoS pathogens. 2010; 6:e1001195. [PubMed: 21124990]
107. Blattner C, et al. Structural Delineation of a Quaternary, Cleavage-Dependent Epitope at the gp41-gp120 Interface on Intact HIV-1 Env Trimers. Immunity. 2014; 40:669–680. [PubMed: 24768348]
108. Yasmeen A, et al. Differential binding of neutralizing and non-neutralizing antibodies to native-like soluble HIV-1 Env trimers, uncleaved Env proteins, and monomeric subunits. Retrovirology. 2014; 11:41. [PubMed: 24884783]
109. Falkowska E, et al. Broadly Neutralizing HIV Antibodies Define a Glycan-Dependent Epitope on the Prefusion Conformation of gp41 on Cleaved Envelope Trimers. Immunity. 2014; 40:657–668. [PubMed: 24768347]
110. Thali M, et al. Characterization of conserved human immunodeficiency virus type 1 gp120 neutralization epitopes exposed upon gp120-CD4 binding. Journal of virology. 1993; 67:3978–3988. [PubMed: 7685405]
111. Guttman M, et al. CD4-Induced Activation in a Soluble HIV-1 Env Trimer. Structure. 2014; 22:974–984. [PubMed: 24931470]
112. Scheid JF, et al. Sequence and structural convergence of broad and potent HIV antibodies that mimic CD4 binding. Science. 2011; 333:1633–1637. [PubMed: 21764753]
113. Walker LM, et al. Broad and potent neutralizing antibodies from an African donor reveal a new HIV-1 vaccine target. Science. 2009; 326:285–289. [PubMed: 19729618]
114. Stanfield RL, Wilson IA. Structural studies of human HIV-1 V3 antibodies. Human antibodies. 2005; 14:73–80. [PubMed: 16720977]
115. Rizzuto CD, et al. A conserved HIV gp120 glycoprotein structure involved in chemokine receptor binding. Science. 1998; 280:1949–1953. [PubMed: 9632396]
116. Guan Y, et al. Diverse specificity and effector function among human antibodies to HIV-1 envelope glycoprotein epitopes exposed by CD4 binding. Proceedings of the National Academy of Sciences of the United States of America. 2013; 110:E69–78. [PubMed: 23237851]
117. Gorny MK, VanCott TC, Williams C, Revesz K, Zolla-Pazner S. Effects of oligomerization on the epitopes of the human immunodeficiency virus type 1 envelope glycoproteins. Virology. 2000; 267:220–228. [PubMed: 10662617]
118. Yuan W, et al. Oligomer-specific conformations of the human immunodeficiency virus (HIV-1) gp41 envelope glycoprotein ectodomain recognized by human monoclonal antibodies. AIDS research and human retroviruses. 2009; 25:319–328. [PubMed: 19292593]
119. Moore PL, et al. Nature of nonfunctional envelope proteins on the surface of human immunodeficiency virus type 1. Journal of virology. 2006; 80:2515–2528. [PubMed: 16474158]
120. Frey G, et al. Distinct conformational states of HIV-1 gp41 are recognized by neutralizing and non-neutralizing antibodies. Nature structural & molecular biology. 2010; 17:1486–1491.
121. Miller MD, et al. A human monoclonal antibody neutralizes diverse HIV-1 isolates by binding a critical gp41 epitope. Proceedings of the National Academy of Sciences of the United States of America. 2005; 102:14759–14764. [PubMed: 16203977]

122. Chen J, et al. Mechanism of HIV-1 neutralization by antibodies targeting a membrane-proximal region of gp41. Journal of virology. 2014; 88:1249–1258. [PubMed: 24227838]

123. Frey G, et al. A fusion-intermediate state of HIV-1 gp41 targeted by broadly neutralizing antibodies. Proceedings of the National Academy of Sciences of the United States of America. 2008; 105:3739–3744. [PubMed: 18322015]

124. Nicely NI, et al. Crystal structure of a non-neutralizing antibody to the HIV-1 gp41 membrane-proximal external region. Nature structural & molecular biology. 2010; 17:1492–1494.

125. Huang J, et al. Broad and potent neutralization of HIV-1 by a gp41-specific human antibody. Nature. 2012; 491:406–412. [PubMed: 23151583]

126. Chakrabarti BK, et al. HIV type 1 Env precursor cleavage state affects recognition by both neutralizing and nonneutralizing gp41 antibodies. AIDS research and human retroviruses. 2011; 27:877–887. [PubMed: 21158699]

127. Ruprecht CR, et al. MPER-specific antibodies induce gp120 shedding and irreversibly neutralize HIV-1. The Journal of experimental medicine. 2011; 208:439–454. [PubMed: 21357743]

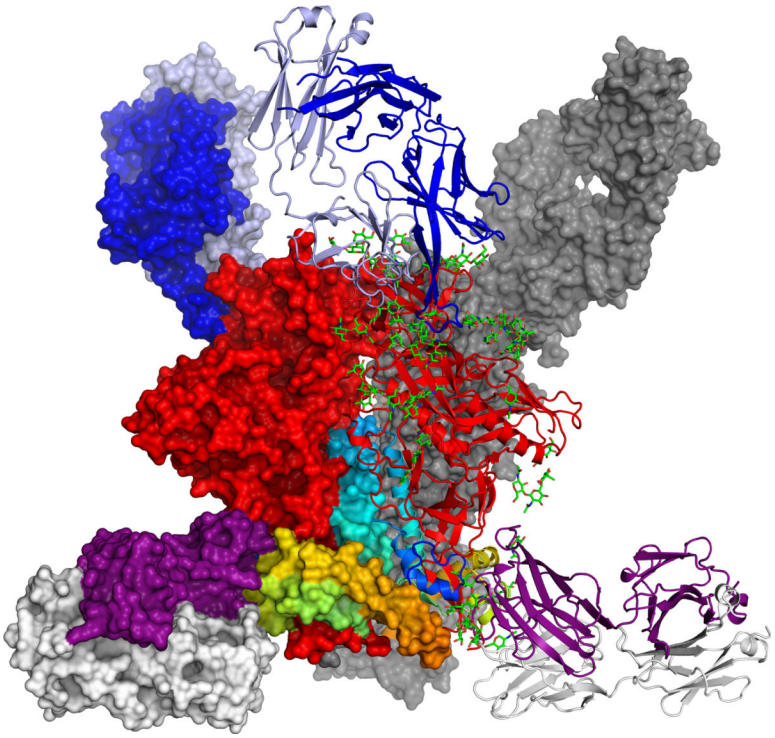

Figure 1. Structure of a prefusion HIV-1-Env trimer bound by PGT122 and 35O22 antibodies

One protomer and associated Fabs is shown in ribbon and stick representation, a second protomer in surface representation, and the third protomer in gray. Residues comprising the refined HIV-1-Env model are displayed on the bar, with beginning and final ordered residue of each segment labeled; vertical lines demark termini of the mature ectodomain subunits; unmodeled regions, residues not present in the BG505 SOSIP.664 construct, and disordered glycans are shown in gray. 35O22 and PGT122 interactions with the HIV-1-Env trimer are shown in Extended Data Fig. 9a-f, and bound versus unbound Fabs are shown in Extended Data Fig. 9g.

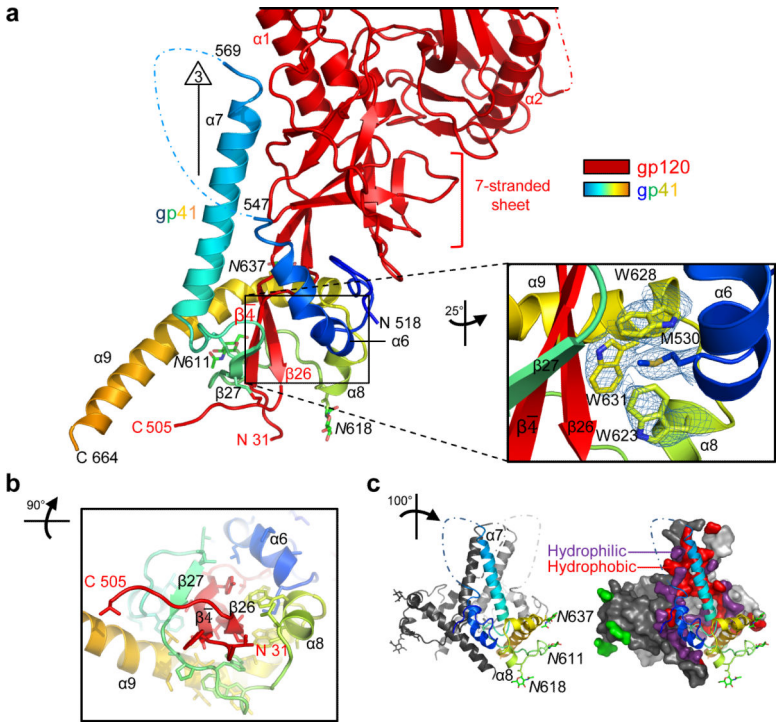

Figure 2. Prefusion structure of gp41

a, gp41 forms a 4-helix collar, which wraps around extended N and C termini of gp120. Both gp120 (red) and gp41 (rainbow from blue to orange) are depicted in ribbon representation, with select residues and secondary structure labeled (additional labels are shown in Extended Data Fig.10). The location of the trimer axis is indicated with triangle-surround "3". The orientation shown here is similar to that of Fig. 1, with perpendicular orientations provided in **b** and **c**. (zoom insert) The gp41 collar is clasped by the insertion of $Met530_{gp41}$ into a tryptophan sandwich and by the complementary dipoles of helices α6 and α8. $2F_o$-F_c electron density for clasp residues is depicted at 1σ. **b**, gp41 holds the N and C termini of gp120 in its hydrophobic core. Coloring and representation are the same as in **a**, excepted that hydrophobic side chains are shown in stick representation and the orientation is rotated 90°, to depict the view from the viral membrane. **c**, gp41-trimer interfaces as viewed from side in ribbon and surface representation. Overall, the prefusion structure of gp41 and its trimeric arrangement appear to have no close structural relatives in the PDB (Supplementary Table 2).

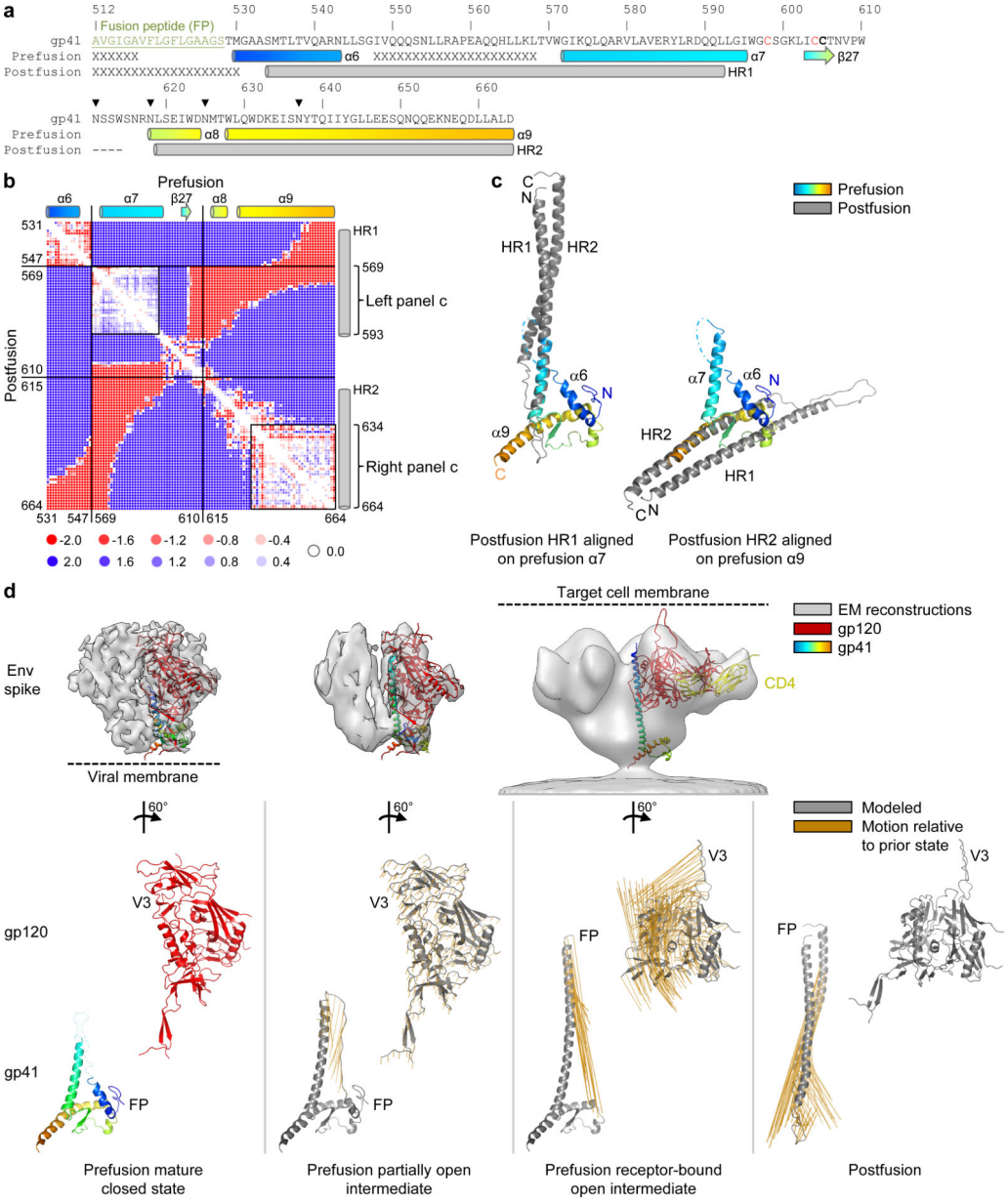

Figure 3. Entry rearrangements of HIV-1 Env

a, BG505 sequence[46] of gp41, with prefusion and postfusion secondary structure. Fusion peptide (FP) is underlined and labeled green. Several postfusion gp41 structures have been determined ranging from a minimal, protease-treated, crystal structure (residues 556_{gp41}-581_{gp41}; 628_{gp41}-661_{gp41}; PDB ID: 1AIK[8]) with 80% sequence identity to BG505[46] to a more complete gp41 structure (residues 531_{gp41}-581_{gp41}; 624-681_{gp41}; PDB ID: 2X7R[24]) and an NMR structure that includes the cysteine loop (residues 539_{gp41}-665_{gp41}; PDB ID: 2EZO[25]) of the simian immunodeficiency virus (SIV), which shares 48% sequence identity with BG505[46] and is substantially similar to the HIV-1 structures (less than 1-Å Cα rmsd between overlapping residues of 1AIK and 2EZO). The postfusion structure utilized here for comparisons was constructed from a chimera of

HIV-1/SIV structures (Extended Data Fig. 3c). **b**, Difference distance analysis[26] of prefusion BG505 and postfusion HIV-1/SIV chimeric gp41. Secondary structure is indicated, along with missing residues of BG505 (548-568) and of SIV (611-614). **c**, Superposition of postfusion gp41 (grey) onto prefusion gp41 (rainbow) for α7 (left) and α9 (right) prefusion helices. **d**, HIV-1-Env entry rearrangements. EM reconstructions (top row) with gp120 (middle) and gp41 (bottom) rearrangements between each conformational state highlighted with orange lines depicting movement of each Cα between conformations. Subunit models are shown in gray with modeling parameters and references provided in Extended Data Table 2. Antigenic recognition of each of these states is shown in Extended Data Fig. 5.

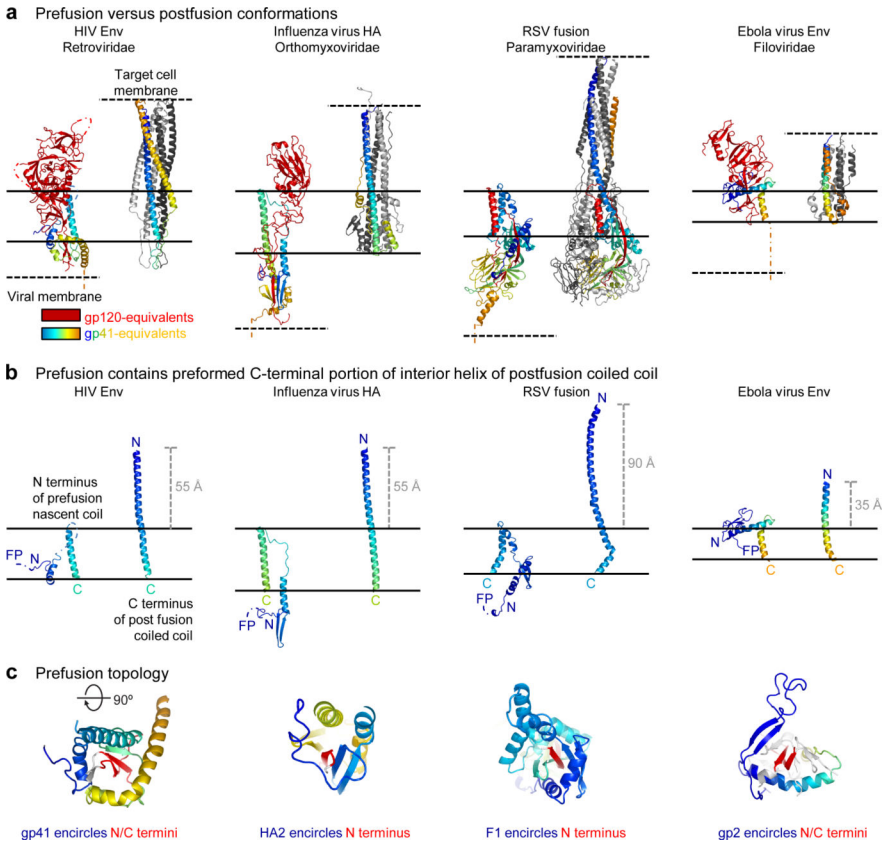

Figure 4. Prefusion HIV-1 gp120-gp41 structure shares conserved structural and topological features with other type I fusion machines

a, Prefusion (left) and postfusion (right) structures. The prefusion structures are shown for a single protomer in ribbon-representation with gp120-equivalent subunits in red, and gp41-equivalent subunits in rainbow (blue to orange). The trimeric postfusion structures are shown with one subunit in rainbow (blue to orange), and the other in light and dark gray. **b**, The C-terminal portion of the preformed interior helix of postfusion coiled-coil from **a** is shown, with fusion peptides (FP) and N and C terminal residues of postfusion coiled-coils labeled, and the distance the inner coiled-coil extends between prefusion and postfusion conformations indicated. **c**, The gp41-equivalents encircle extended β-strands of their gp120-equivalent partners. Ribbon representations are shown looking towards the viral membrane. With influenza, it is only the N terminus of the gp120-equivalent (HA1) that is wrapped by the gp41-equivalent (HA2), with the N terminus of HA2 completing about 20% more than a single encirclement. With RSV, it is also only the N terminus of the gp120 equivalent (F2) that is wrapped by the gp41-equivalent (F1), and the termini do not have to be expelled to transition to the postfusion form. With Ebola, the gp41-equivalent (gp2) wraps both N and C termini-strands of the gp120-equivalent (gp1), completing about 70% of a single encirclement. Such encirclement likely helps capture the energy of prefusion folding, which is released during the postfusion transition to power membrane fusion.

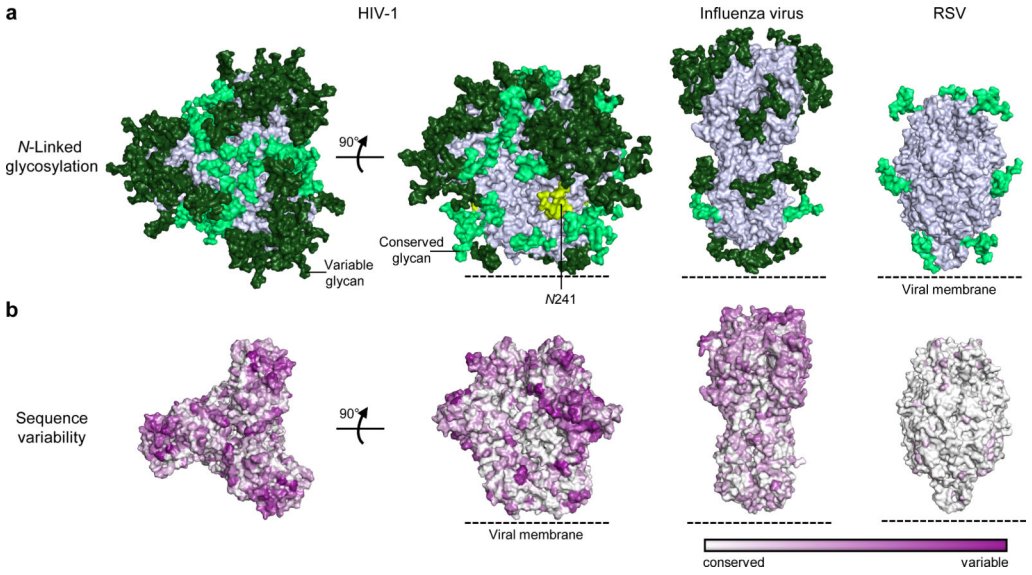

Figure 5. Fully assembled shield revealed by prefusion HIV-1 gp120-gp41 trimer

a, Glycan shield. Env *N*-linked glycans are depicted in light green (conserved; greater than 90% conservation) or dark green (variable; less than 90% conservation) on the prefusion mature closed Env structures for BG505 strain of HIV-1 (left), influenza virus H3 hemagglutinin (PDB ID: 2YP7) (middle), and RSV fusion glycoprotein subtype A (PDB ID: 4JHW) (right). A conserved glycan at residue 241_{gp120} not present in the BG505 sequence is shown in yellow-green. **b**, Sequence variability.

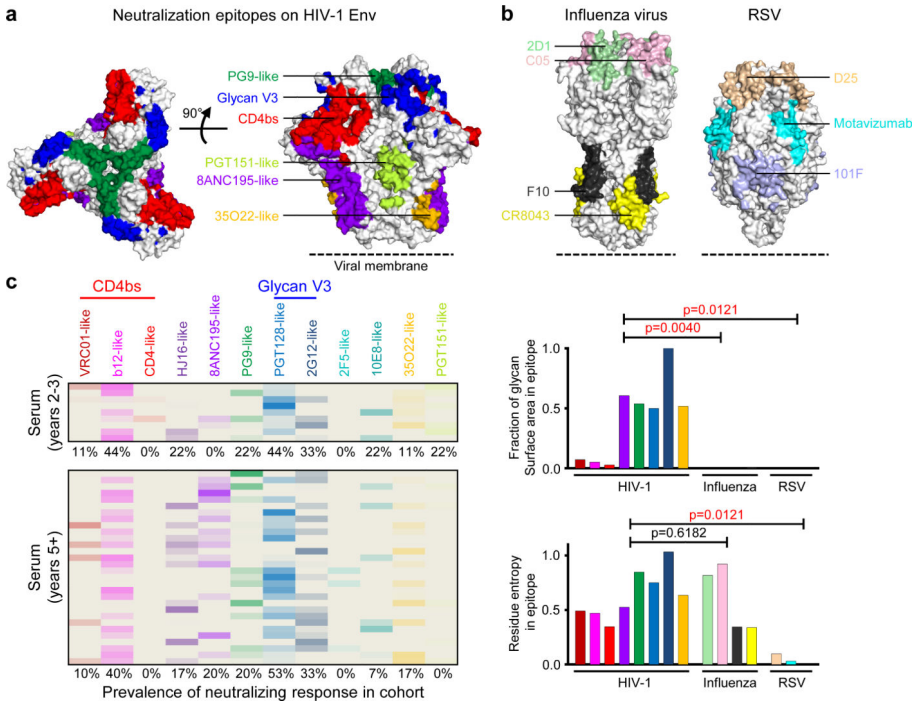

Figure 6. Location and prevalence on the HIV-1-Env spike of neutralizing responses identified serologically from cohorts, 2-3 and 5+ years post-infection

a, The location of the neutralization epitopes for broadly neutralizing antibodies is depicted on the prefusion mature closed Env spike with red for CD4-binding-site-directed antibody specificities (VRC01-, b12-, CD4-, and HJ16-like), purple for 8ANC195-like, green for V1V2-directed (PG9-like), blue for glycan-V3 specificities (PGT128- and 2G12-like), orange for 35O22-like specificities, and green-yellow for PGT151-like specificities. **b**, (top) Broadly neutralizing epitopes on influenza virus hemagglutinin (left, PDB ID: 2YP7) and RSV fusion glycoprotein (right, PDB ID: 4JHW). (bottom) Glycan-surface area and residue entropy of antibody epitopes for HIV-1, influenza, and RSV with bars colored according to epitopes shown in **a** and **b** (except for epitopes not present in SOSIP.664 or where there is no atomic level definition). **c**, Neutralization fingerprint. For each serum, the predicted neutralization prevalence for each of the 12 antibody specificities is shown based on neutralization of 21 diverse HIV-1 strains (Extended Data Fig. 8).